Vehicular Trajectory Estimation Utilizing Slip Angle Based on GNSS Doppler/IMU

Kanamu Takikawa (193432010@ccmailg.meijo-u.ac.jp)
Meijo University Faculty of Science and Technology Graduate School of Science and Technology: Meijo Daigaku Rikogakubu Daigakuin Rikogaku Kenkyuka https://orcid.org/0000-0001-7773-6962

Yoshiki Atsumi
Meijo University Faculty of Science and Technology Graduate School of Science and Technology: Meijo Daigaku Rikogakubu Daigakuin Rikogaku Kenkyuka

Aoki Takanose
Meijo University Faculty of Science and Technology Graduate School of Science and Technology: Meijo Daigaku Rikogakubu Daigakuin Rikogaku Kenkyuka

Junichi Meguro
Meijo University: Meijo Daigaku

Research Article

Keywords: Vehicle Trajectory, Two-wheel model, Autonomous Driving Systems, Multi-GNSS, Urban area

Posted Date: October 13th, 2020

DOI: https://doi.org/10.21203/rs.3.rs-90799/v1

Version of Record: A version of this preprint was published on February 16th, 2021. See the published version at https://doi.org/10.1186/s40648-021-00195-4.

Vehicular Trajectory Estimation utilizing Slip Angle based on GNSS Doppler/IMU

Kanamu Takikawa [*1], Meijo University, 193432010@ccmailg.meijo-u.ac.jp
Yoshiki Atsumi [1], Meijo University
Aoki Takanose [1], Meijo University
Junichi Meguro [2], Meijo University

Key Words: Vehicle Trajectory, Two-wheel model, Autonomous Driving Systems, Multi-GNSS, Urban area

Abstract— **Accurate vehicular trajectory estimation is important for the recently developed autonomous driving systems. As the accuracy of the vehicular trajectory estimation is reduced with the slippage that occurs during turning, we propose a method in this study to accurately estimate the trajectory of a vehicle, focusing on the slip angle estimation. Although the two-wheel model is used as a general concept slip angle estimation, the accurate estimation of the parameters was difficult using the conventional methods. Therefore, a global navigation satellite system (GNSS) Doppler was used for parameter estimation. In addition, the roll angle was estimated as it occurs during turning and affects the slip angle of the vehicle. Specifically, we verified the improvement in accuracy of the vehicular trajectory estimation using the cost-effective GNSS Doppler/inertial measurement unit.**

I. Introduction

Highly accurate vehicular trajectory estimation has become imminently important for automated vehicles and advanced driver assistance systems that have been developed in the recent years [1]. Accurate trajectory information has been used in various studies such as constraints for position estimation, 3-D mapping for automated vehicles, route planning, and vehicular control [2-7]. The trajectory estimation accuracy of an automated vehicle should be accurate to one tire with a 2-D error of 0.30 m/100 m. Moreover, conventional automated vehicles often use global navigation satellite systems/intertial measurement unit (GNSS/IMU) systems with expensive sensors, such as fiber-optic gyros, to achieve the required accuracy. However, the cost of using these expensive sensors is an issue. Therefore, the method proposed in this study aims to achieve accurate trajectory estimation using inexpensive sensors. A difference is known to occur between the directions of the velocity vector and the attitude angle (slip angle) when the vehicle turns. Therefore, the slip angle estimation is generally carried out using a two-wheeled model to improve the accuracy of vehicular trajectory estimations [8]. However, the two-wheeled models require one-by-one estimation of multiple parameters, which imparts error biases and

[1]*Correspondence: 1934320010@ccmailg.meijo-u.ac.jp
[1]Division of Mechatronics Engineering, Graduate School of Science and Technology, Meijo University, Shiogamaguchi 1-501, Tenpaku-ku, Nagoya, Aichi 468-0073, Japan
Full list of author information is available at the end of the article

makes the accurate estimation of vehicular trajectory difficult.

Therefore, the proposed method uses a GNSS Doppler to ensure the high-accuracy estimation of vehicular trajectories by compensating for slip angles occurring in a motorcycle model. In order to confirm the effectiveness of the correction of the slip angle on the trajectory, the accuracy of the trajectory was determined in the direction straight down the road with data acquired and evaluated from two different environments.

II. Related Prior Research

A. Overview of conventional trajectory estimation

Generally, conventional vehicle trajectory estimation utilizes IMUs and wheel speedometers [1,9,10]. First, the trajectory can be broken into its east and north components, and the trajectory at time t can be expressed using Equations (1) and (2) as follows.

$$T_{\mathrm{East}}{}^{t} = T_{\mathrm{East}}{}^{t-1} + V \cdot \cos(\psi + \beta) \cdot dt \quad (1)$$

$$T_{\mathrm{North}}{}^{t} = T_{\mathrm{North}}{}^{t-1} + V \cdot \sin(\psi + \beta) \cdot dt \quad (2)$$

V: velocity, ψ: heading angle, β: slip angle.

Here, the heading angle ψ is expressed in the following equation (3) using the yaw rate $\dot{\psi}$:

$$\psi^{t} = \psi^{t-1} + (\dot{\psi}^{t} + \delta\dot{\psi}) \cdot \frac{1}{\cos(\theta) \cdot \cos(\varphi)} \cdot dt \quad (3)$$

$\dot{\psi}$: yaw rate, θ: pitch angle, φ: roll angle.

Equation (3) considers the error in the IMU yaw rate $\dot{\psi}$ with an offset of $\delta\dot{\psi}$. Furthermore, Equation (4) presents the consideration of including the scale factor of wheel speed and the effect of the longitudinal slope of the road with respect to V.

$$V = SF \cdot V_{\mathrm{can}} \cos(\theta) \quad (4)$$

V_{can}: CAN-bus Velocity, SF: Scale Factor Error.

Using Equations (1)–(4), the vehicle trajectory can be calculated from the output of the IMU using the wheel speed. Therefore, the elements of trajectory that need to be estimated are ψ, β, $\delta\dot{\psi}$, SF, φ, and θ. Among them, a highly accurate estimation method has been proposed for ψ, $\delta\dot{\psi}$, SF, and θ [1]; therefore, the estimation of the roll angle φ and slip angle β remains unfulfilled. Thus, this study focuses to estimate the slip angle, which is more accurate along the direction of the road and has a greater correction effect.

B. Previous studies on slip angle estimation

The equipment required to directly measure the slip angle of a vehicle is expensive and difficult to install in a vehicle [11]. Consequently, estimation is often preferred and performed, where the direct integration method [8] and the linear observer estimation method [12] are used as typical methods for conventional estimation of the slip angle. However, the direct integration method poses a problem of accumulation of noise and offset in the sensor detections owing to the inclusion of an integrator, and the error increases with time. On the contrary, the linear two-degree-of-

freedom model (two-wheel model) of the linear observer estimation method is used to construct the settings for an observer to conduct the estimation (Figure 1). In the two-wheel model, both the left and right front tires of a four-wheeler vehicle are assumed to have identical slip angles and are treated as equivalent to those of the two wheels. Equation (5) depicts the relationship between the slip angle at the center of gravity β and the parameters of the vehicle.

$$\beta = \left(\frac{1 - \frac{mL_f}{2LL_rK_r}V^2}{1 - \frac{m}{2L^2}\left(\frac{L_fK_f - L_rK_r}{K_fK_r}\right)V^2} \right) \frac{L_r\delta}{L} \qquad (5)$$

m: vehicle weight, L: distance between front and rear wheels, L_f: distance between center of gravity of front wheel, L_r: distance between center of gravity and the rear wheels of the vehicle, V: velocity, K_f: front wheel cornering power, K_r: rear wheel cornering power , δ: steering angle.

Here, the linear observer estimation method measures the parameters required for the estimation of the slip angle from the inertial sensor measurements [11-12]. However, individual measurements of these parameters lead to a problem of error bias. In particular, the coefficients K_f and K_r are difficult to measure accurately owing to various factors such as the effect of deformed tires. In addition, there are limitations such as the need for accurate estimation of the steering angle and the requirement for tuning for each vehicle [13-15].

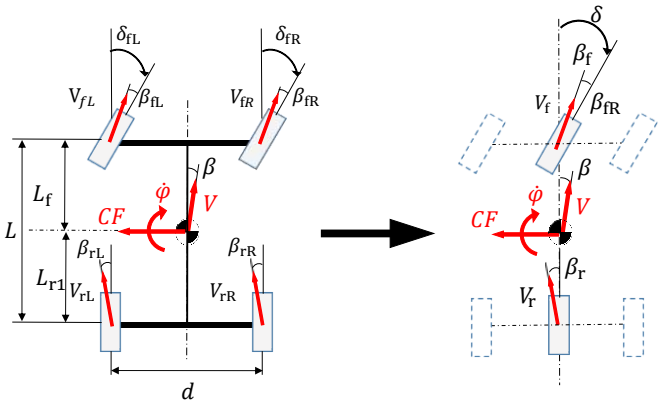

Figure 1 Two-wheel model

III. Our Proposal

A. Overview of the slip angle estimation

The proposed method aims to resolve the limitation of determining the parameters of the two-wheeled model for the estimation of the slip angle β by the estimating parameters automatically using GNSS Doppler. In addition, the proposed method eliminates the term of steering angle in the two-wheel motorcycle model, and thus does the estimation of steering angle is not required. The proposed method is expected to increase the accuracy of the slip angle estimation to an extent of validating the two-wheel model. Figure 2 shows an overview of the method.

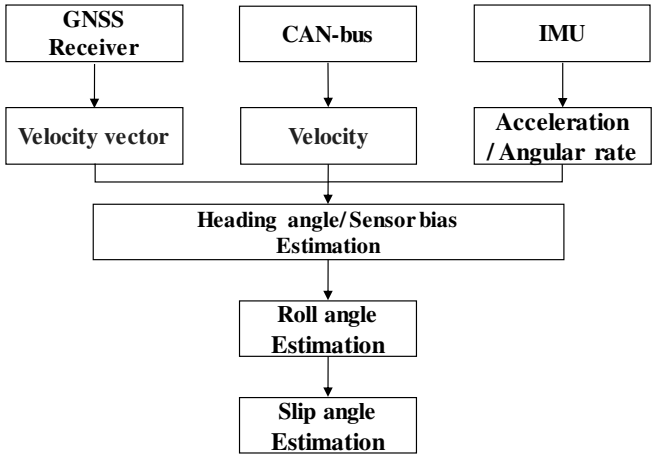

Figure 2 Overview of the proposal

In the two-wheel model, the yaw rate $\dot{\psi}$ can be expressed by Equation (6) [12] as follows.

$$\dot{\psi} = \left(\frac{1}{1 - \frac{m}{2L^2}\left(\frac{L_f K_f - L_r K_r}{K_f K_r}\right) V^2} \right) \frac{V\delta}{L} \quad (6)$$

Therefore, Equations (5) and (6) can be combined to obtain the relationship between β and $\dot{\psi}$ as given by Equation (7).

$$\beta = \dot{\psi}\left(\frac{L_\mathrm{r}}{V} - \frac{mL_\mathrm{f}}{2LK_\mathrm{r}}V\right) \quad (7)$$

However, the above equation represent the slip angle β at the center of gravity. The slip angle β_r at the center of the rear wheel axle is given by equation (8).

$$\beta_\mathrm{r} = \beta - \frac{L_\mathrm{r}}{V}\dot{\psi} \quad (8)$$

Combining Equations (7) and (8), we can obtain equation (9) as

$$\beta_\mathrm{r} = -\frac{mL_\mathrm{f}}{2LK_\mathrm{r}}\dot{\psi}V \quad (9)$$

As all the parameters in Equation (9) are fixed and constant parameters, except for $\dot{\psi}$ and V, they can be comprehensively represented as the gain K in the following equation (10):

$$\beta_\mathrm{r} = -K\dot{\psi}V \quad (10)$$

where $\dot{\psi}V$ is the product of the yaw rate and velocity and refers to the centrifugal acceleration, so it can be summarized as G_y in Equation (11).

$$\dot{\psi}V = G_y \quad (11)$$

Therefore, Equation (11) simplifies to Equation (12) .

$$\beta_\mathrm{r} = -K \cdot G_y \quad (12)$$

Furthermore, during motion of the vehicle, the component of gravitational acceleration g for the roll angle needs to be considered for Equation (12) because the component of gravity is included at the time of roll angle generation. Figure 3 shows the relationship between the roll angle and its occurrence. The

relationship between the roll angle φ and the lateral acceleration G_y is expressed in Equation (13).

$$G_y = \dot{\psi} \cdot V - g \cdot \sin\varphi \tag{13}$$

Substituting G_y from Equation (13) to Equation (12), we obtain Equation (14) as:

$$\beta_r = -K(\dot{\psi} \cdot V - g \cdot \sin\varphi) \tag{14}$$

Therefore, the sine component of the roll angle is necessary for the estimation of the slip angle from Equation (14), which is estimated in the next subsection.

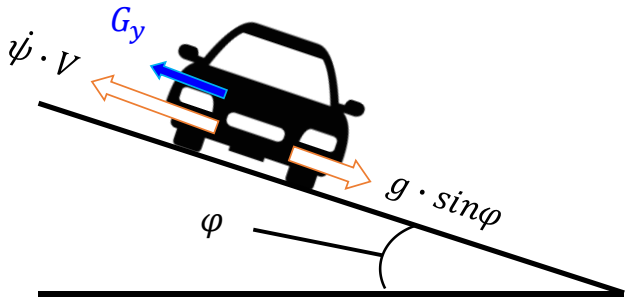

Figure 3 Effect of road lateral gradient

B. Roll angle estimation

The roll angle can be estimated with the formula presented by Tseng et al. [16]:

$$\varphi = arcsin\left(\frac{V}{g} \cdot \dot{\psi} - \frac{G_y}{g}\right) \tag{15}$$

Moreover, the transverse acceleration G_y can be measured from the IMU, and for the error in acceleration of the IMU as $\delta {G_y}^{\text{imu}}$, Equation (15) can be expressed as Equation (16).

$$\varphi = arcsin\left(\frac{V}{g} \cdot \dot{\psi} - \frac{{G_y}^{\text{imu}} + \delta {G_y}^{\text{imu}}}{g}\right) \tag{16}$$

Assuming that Equation (16) holds true, the roll angle φ can be estimated upon the correction of $\delta {G_y}^{\text{imu}}$.

Therefore, this study proposes a method for estimating the lateral acceleration error using the relationship between the variation in the heading angle ψ at certain intervals and the integration of the yaw rate $\dot{\psi}$ with the roll angle φ. The relationship between the variation of heading angle at certain intervals and the integration of the yaw rate $\dot{\psi}^{2D}$ as viewed from the horizontal plane can be expressed by equation (17).

$$\psi^{t+k} - \psi^{t} = \int_{t}^{t+k} \dot{\psi}^{2D}\, dt \tag{17}$$

However, the roll angle φ needs to be considered with respect to the yaw rate in case of a lateral slope on the road surface.

$$\psi^{t+k} - \psi^{t} = \int_{t}^{t+k} \dot{\psi} \cdot \frac{1}{\cos(\varphi)}\, dt \tag{18}$$

Therefore, the expression of roll angle in Equation (16) can be substituted into the above Equation (18) to obtain the following Equation (19).

$$\psi^{t+k} - \psi^{t} = \int_{t}^{t+k} \dot{\psi} \cdot \frac{1}{\cos\left\{arcsin\left(\frac{V}{g} \cdot \dot{\psi} - \frac{{G_y}^{\text{imu}} + \delta {G_y}^{\text{imu}}}{g}\right)\right\}} dt \quad (19)$$

Equation (19) shows the relationship between the azimuthal angle and the transverse acceleration error at certain intervals. Therefore, the accurate evaluation of the lateral acceleration error through Equation (19) can be used to accurately estimate the roll angle through Equation (16).

In this study, we determined $\delta {G_y}^{\text{imu}}$ by utilizing the heading difference between the left and right sides of Equation (19). By varying the value of $\delta {G_y}^{\text{imu}}$ in Equation (19), we search for cases where the heading difference is zero or closest to zero, and thus analytically determine $\delta {G_y}^{\text{imu}}$. In Equation (19), the heading angle ψ can be estimated by using the GNSS Doppler/IMU [1,17,18], the velocity V can be measured by the wheel speed sensor, and ${G_y}^{\text{imu}}$ can be measured by the IMU, so only $\delta {G_y}^{\text{imu}}$ remains unknown, for which the estimation can be made. The transverse acceleration error $\delta {G_y}^{\text{imu}}$ cannot be estimated using Equation (19) when entire right-hand side of the equation becomes zero for 0 rad/s yaw rate $\dot{\psi}$. Therefore, the computation was performed only at the point where the curve turned once. In this study, we used data for 100 s with k = 100. Figure 4 portrays the variation in the heading difference between the left and right sides for different values of $\delta {G_y}^{\text{imu}}$ within –1.5 to 1.5 m/s^2 according to Equation (19). As shown, the variation of $\delta {G_y}^{\text{imu}}$ produced quadratic curves with inflection points indicating minimum differences between the left and right sides. As each of these inflection points was calculated at a different position on a curve, the average of these values were considered to neutralize the transverse acceleration error $\delta {G_y}^{\text{imu}}$. This estimate did not considerably vary over time so determining sequence was not necessary. Therefore, the real-time position estimation can be performed right after conducting the calibration run estimating the initial position. For this dataset, we considered 0.25 m/s^2 as the estimated value.

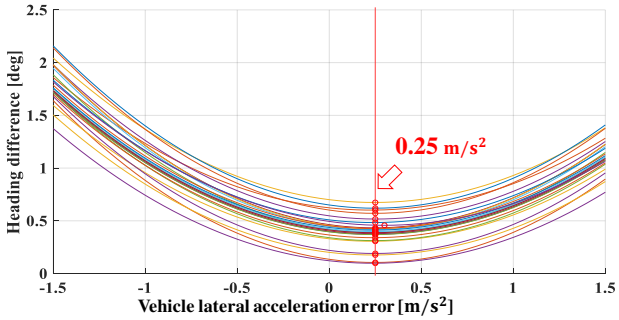

Figure 4 Estimation results of the lateral acceleration error

C. Parameter estimation for two-wheel model using GNSS Doppler

Figure 5 presents the relationship between the slip angle and lateral acceleration according to Equation

(14) for a distance of approximately 5 km around the urban area (Odaiba, Tokyo, Japan). The slip angle and the lateral acceleration were measured by Applanix POSLV220, which is known as a high-precision GNSS/IMU system [19]. The correlation between the slip angles with lateral acceleration can be observed from Figure 5, where the slope represents the gain K from equation (14). Therefore, the slip angle can be estimated by evaluating this relationship.

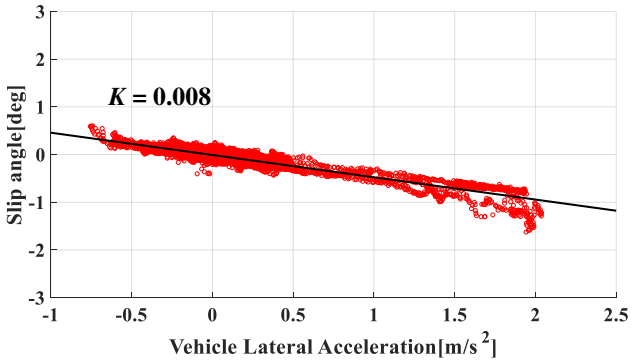

Figure 5 Correlation between slip angle and lateral acceleration (POSLV220)

On the contrary, the velocity vector and attitude angle can be estimated by utilizing the GNSS Doppler [20] and combining the IMU with it [1], respectively. Therefore, this study proposes a method to approximate the variation in attitude angles using the GNSS Doppler/IMU and evaluate the first-order approximation of velocity vectors using the GNSS Doppler with the least-squares method, where the slope of the first-order equation is represented by the gain K. An overview of the proposed method has been presented in Figure 6, where β_r was accumulated according to Equation (20) by calculating the difference between the directions obtained from the GNSS Doppler/IMU $H_{\text{Doppler/IMU}}$ and the GNSS Doppler H_{Doppler} at the curve. Moreover, thresholds were set for speed and storage of data beyond a certain speed owing to the higher speed range of the moving object and the higher accuracy of the GNSS Doppler [1,17,18,20].

$$\beta_r \,{}^{\text{Doppler/IMU}}_{\text{Doppler}} = H_{\text{Doppler/IMU}} - H_{\text{Doppler}} \qquad (20)$$

The gain K was estimated using the above equation with the relationship between the accumulated slip angle and lateral acceleration; the gain K shown in Figure 7 can be estimated without using a high-precision GNSS/IMU.

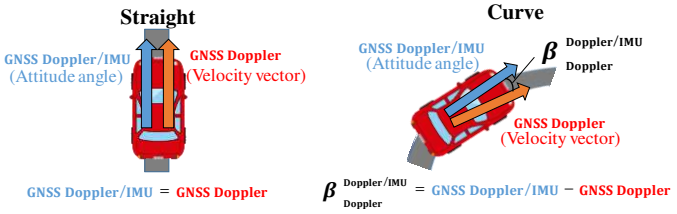

Figure 6 Overview of the slip angle

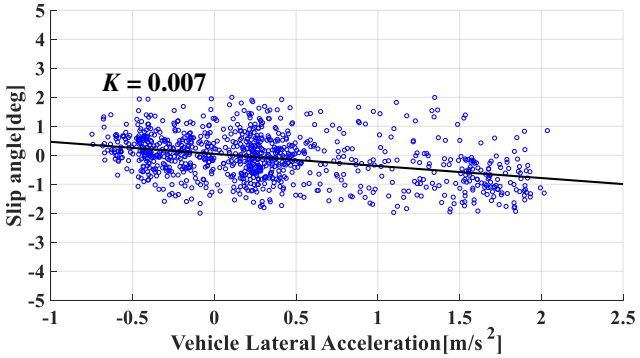

Figure 7 Relationship between slip angle and lateral acceleration using GNSS/Doppler

IV. Evaluation tests

The evaluation tests were conducted on a 5-km course in an urban street (Odaiba, Tokyo, Japan) and a 14-km course on an urban highway (Tokyo Metropolitan Expressway) with a lateral gradient; the courses are shown in Figure 8. The U-blox M8T with a GPS+BeiDou+Galileo+QZSS satellite system was used as a GNSS receiver with a reception period of 10 Hz. The MEMS IMU on the TAG264 of Tamagawa Seiki was used with an acquisition period of 50 Hz. An Applanix POSLV220 was used as the reference equipment for an accurate evaluation. Table 1 lists the sensors and the reference POSLV220 used in this evaluation, where a significant difference can be seen in the cost of our proposed sensor scheme with that of the reference model.

Table 1 Equipment used for evaluation

	Sensor	Product name	Cost (US$)
Proposal	GNSS Receiver	Ublox M8T(10Hz)	100
	GNSS Antenna	Tallysman TW2710	100
	MEMS IMU	Tamagawa AU7554(50Hz)	500
Reference	GNSS Receiver, GNSS Antenna, 3-axis FOG	Applanix POSLV220	100000

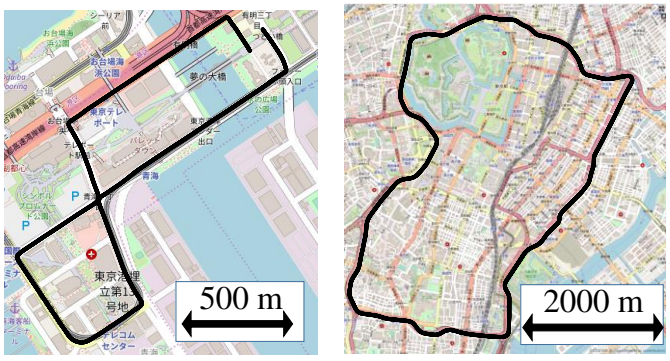

a) Urban street **b) Urban highway**

Figure 8 Evaluation fields [“© OpenStreetMaps”]

A. *Roll angle estimation results*

The roll angles estimated using the lateral acceleration error δG_y with our proposed method is shown in Figures 9 and 10 for the urban street and highway, respectively. In addition, the reference (POSLV220) model measurements along with the raw roll angle estimation (Equation (16)) data without the correction of δG_y (No sensor correction) are presented in these figures for comparison. Furthermore, Figures 11 and 12 show the difference between errors under “No sensor correction” and “Proposal” of the estimated roll angles for the urban street and highway, respectively. Thus, Figures 9–12 show that the proposed method can negate the offsetting error and produces results close to the reference. Tables 2 and 3 show the errors in the estimated roll angles. From Tables 2 and 3, it can be observed that the mean error was improved by the correction of the lateral acceleration error estimated by the proposed method for both the courses.

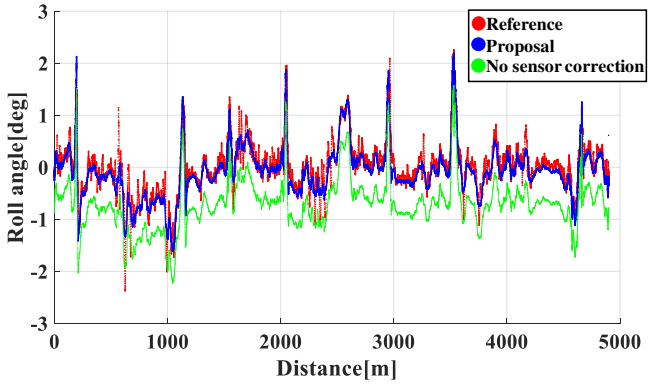

Figure 9 Estimated roll angle (Urban street)

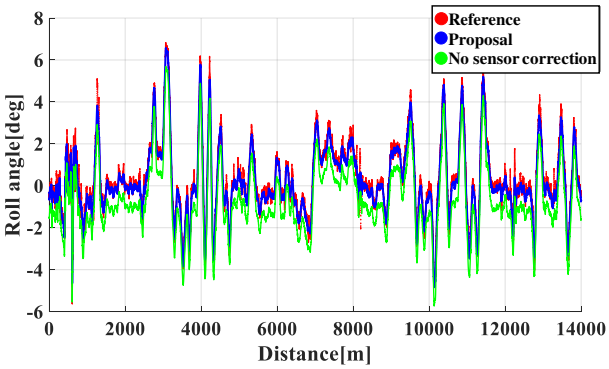

Figure 10 Estimated roll angle (Urban highway)

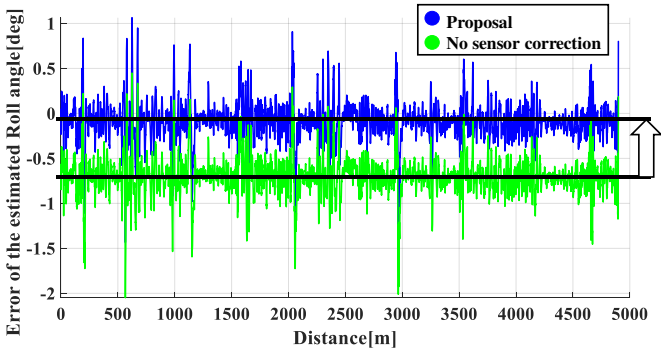

Figure 11 Error of estimated roll angle (Urban street)

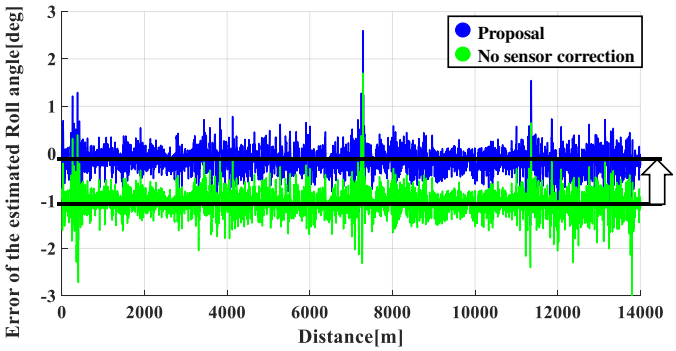

Figure 12 Error of estimated roll angle (Urban highway)

Table 2 Error of estimated roll angle (Urban street)

Error	Average[deg]	Standard deviation[deg]
Proposal	–0.09	0.22
No sensor correction	–0.71	0.22

Table 3 Error of estimated roll angle (Urban highway)

Error	Average[deg]	Standard deviation[deg]
Proposal	–0.17	0.29
No sensor correction	–1.06	0.29

B. Slip angle estimation results

The slip angles estimated using the proposed method are shown in Figures 13 and 14 for the urban street and highway, respectively. These figures prove that the estimated slip angles were close to the reference model for both the courses. Furthermore, the difference between the reference and estimated slip angles are presented in Figures 15 and 16; the error in the estimated slip angle is shown in Table 4.

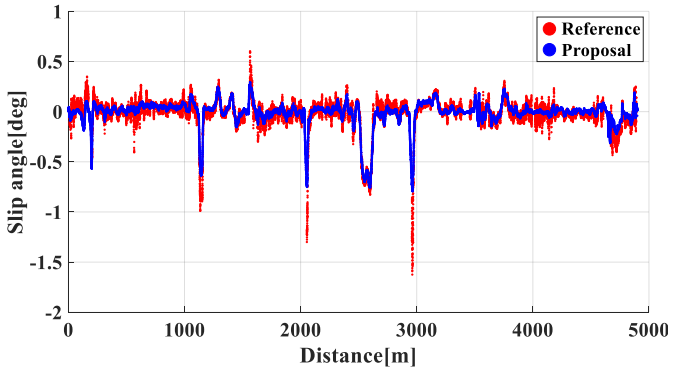

Figure 13 Estimated slip angle (Urban street)

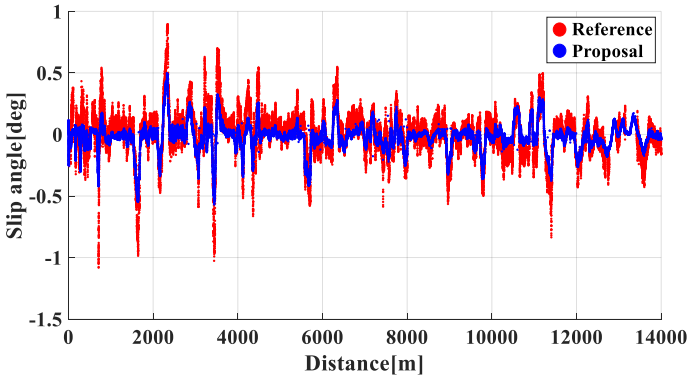

Figure 14 Estimated slip angle (Urban highway)

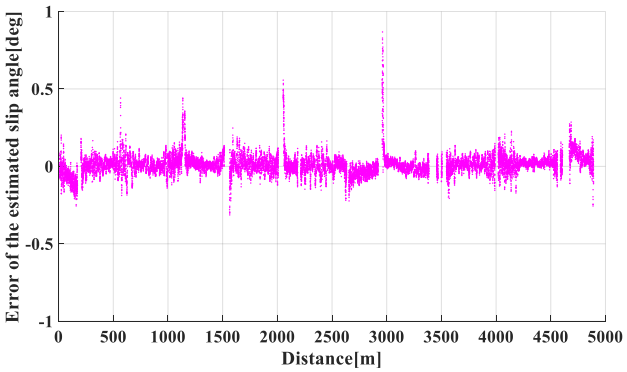

Figure 15 Error of estimated slip angle (Urban street)

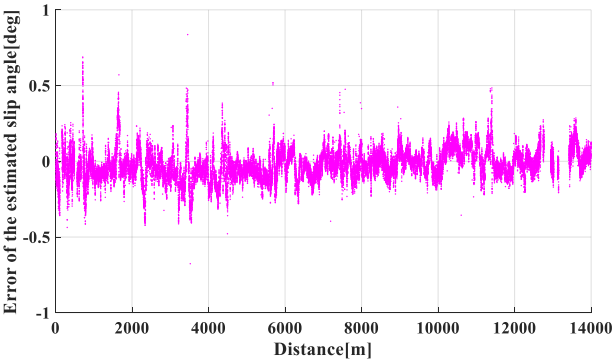

Figure 16 Error of estimated slip angle (Urban highway)

Table 4 Error of estimated slip angle

Error	Average[deg]	Standard deviation[deg]
Urban street	0.01	0.07
Urban highway	–0.01	0.10

C. Trajectory estimation results

Thereafter, the effect of the slip angle correction on the trajectory was evaluated. Figure 17 shows the results of using the corrected slip angle estimation for the trajectory obtained from the conventional method [1,4] at the urban street shown in Figure 8a. The trajectory before and after the slip angle correction is shown in the inset of Figure 17, compared with the trajectory drawn from the starting point aligned to the reference. Figure 17 further shows that the trajectory beyond the turn of curve approached the reference model by correcting the slip angle, which improved the accuracy of the proposed model.

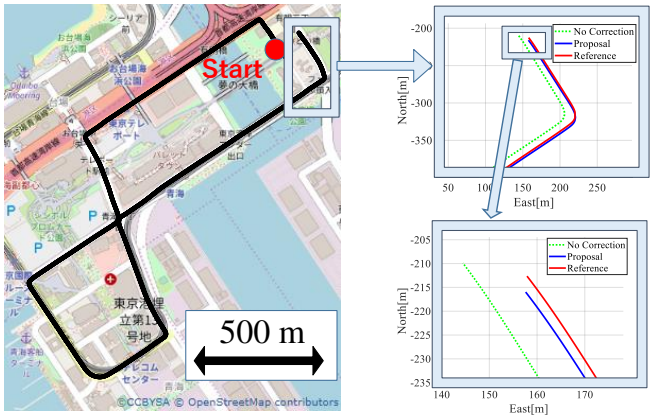

Figure 17 Effect of slip angle correction (Urban street)

In this study, we evaluated the error every 10 m in the trajectory for every 100 m in the direct direction of the road on the urban street and highway. The trajectory was set according to the wheel speed, IMU, and slip angle after aligning the POSLV220 only to the base point. Figure 18 shows an overview of the evaluation test; Figures 19 and 20 show the results of the evaluation, where the accuracy of the trajectory was improved on both the urban street and the highway. In particular, the accuracy of the trajectory—at an error of 30 cm—was approximately 10% higher than that before the correction (no correction). Moreover, the estimation accuracy was improved by considering the roll angle in Equation (14), as compared to excluding the roll angle φ in the given equation. The effect of considering the roll angle was particularly pronounced

on the urban highway that has a large number of lateral slopes.

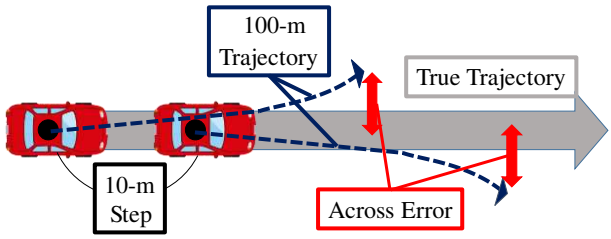

Figure 18 Overview of trajectory evaluation

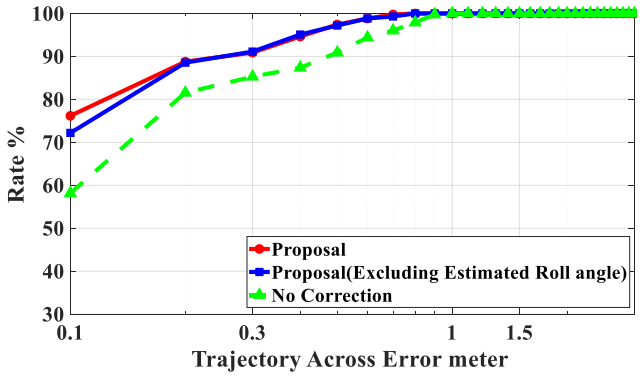

Figure 19 Evaluation of vehicle trajectory (Urban street)

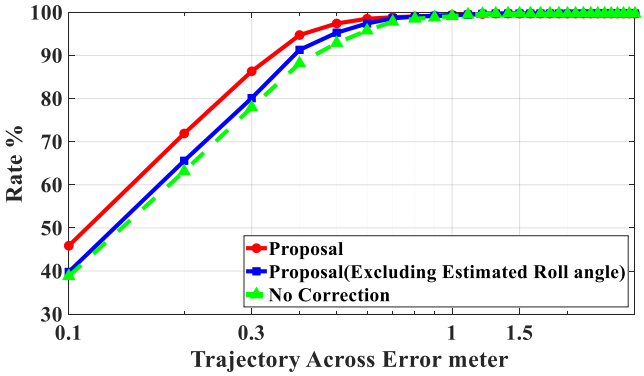

Figure 20 Evaluation of vehicle trajectory (Urban highway)

V. CONCLUSIONS

The purpose of this study was to improve the accuracy of vehicular trajectory, which is an important factor of automatic vehicle driving. Thus, we focused on the accurate estimation of the slip angle, which is a particular challenge in vehicular trajectory estimation. A linear observer estimation method using a two-wheeled model constitutes a typical conventional method for slip angle estimation. These methods facilitate one-by-one estimation of the parameters of the two-wheeled model, thus creating a problem of error bias.

Therefore, in this study, the two-wheel motorcycle model equation for the position of center of gravity was replaced by that for the center of the rear axle slip angle, and the parameters of the motorcycle model were collectively estimated as a gain *K*. This allowed the automatic estimation of parameters and ensured the removal of the steering angle term that was difficult to measure. We utilized the GNSS Doppler/IMU and GNSS Doppler to estimate the gain *K*. The difference between the attitude angles measured by the GNSS Doppler/IMU and the velocity vectors measured by the GNSS Doppler from the motorcycle model was first-order approximated by the least-squares method, and the slope of the first-order equation was defined as the gain *K*. By accounting the effect of the roll angle for the estimation of the gain *K*, a highly accurate slip angle estimation was performed. The roll angle estimation was based on the relationship of the integrated yaw-rate value and the variation of the attitude angle during a certain time period. This study enabled the estimation of the slip angle without the need for the observer and vehicle-specific tuning, and allowed the correction of

slip to be easily incorporated into the trajectory estimation.

The effectiveness of the slip angle correction for the vehicular trajectory was confirmed in the evaluation test. The experiments were conducted on a standard urban (street) course and a high-speed (highway) course that was prone to lateral gradients; the error rates of the 100-m trajectory for both courses were improved by about 10% to cover within 30 cm. The consideration of roll angle improved the accuracy of the estimation, and its effectiveness was especially significant on a course with numerous lateral slopes such as the urban highway.

In this study, an off-line processing was used to improve the accuracy of the trajectory estimation by estimating a highly accurate slip angle. This was effective for off-line use of trajectories such as the creation of 3-D maps for automated driving. As the theoretical capability of the proposed model has been verified for real-time use, we will continue to improve the algorithm for real-time implementation to further improve the usability of the proposed model.

Acknowledgements

Not applicable.

Authors' contributions

KT made a central contribution to the writing of the manuscript by proposing methods, conducting experiments, and analyzing data. All authors read and approved the final manuscript.

Funding

Not applicable.

Availability of data and materials

Not applicable.

Competing interests

The authors declare that they have no competing interests.

Author details

[1] Division of Mechatronics Engineering, Graduate School of Science and Technology, Meijo University, Shiogamaguchi 1-501, Tenpaku-ku, Nagoya, Aichi 468-0073, Japan

[2]Associate Professor with the Department of Mechatronics Engineering, Faculty of Science and Technology, Meijo University. (e-mail: meguro@meijo-u.ac.jp).

REFERENCES

[1] Meguro J, Arakawa T, Mizutani S, Takanose A (2018) Low-cost Lane-level positioning in Urban Area Using Optimized Long Time Series GNSS and IMU Data. In: 2018 21st International Conference of Intelligent Transport Systems (IEEE ITSC), Maui, HI, pp. 3097–3104, 2018. doi: 10.1109/ITSC.2018.8569565.

[2] Ulbrich F, Rotter S, Goehring D, Rojas R (2016) Extracting Path Graphs from Vehicle Trajectories. In: 2016 IEEE Intelligent Vehicle Systems (IV), Gothenburg, Sweden, pp. 1260–1264, 2016. doi: 10.1109/IVS.2016.7535552.

[3] Mukherjee S, Wang S, Wallace A (2020) Interacting Vehicle Trajectory Prediction with Convolutional Recurrent Neural Networks. In: 2020 IEEE International Conference on Robotics and Automation (ICRA), Paris, France, pp. 4336–

4342, 2020. doi: 10.1109/ICRA40945.2020.9196807.

[4] Kurzer K, Engelhorn F, Zollner JM (2018) Decentralized Cooperative Planning for Automated Vehicles with Continuous Monte Carlo Tree Search. In: 2018 21st International Conference on Intelligent Transportation Systems (ITSC), Maui, HI, pp. 452–459, 2018. doi: 10.1109/ITSC.2018.8569988.

[5] Ljungqvist O, Axehill D, Pettersson H (2020) On sensing-aware model predictive path-following control for a reversing general 2-trailer with a car-like tractor. IEEE ICRA arXiv:2002.06874

[6] Buckman N, Pierson A, Karaman S, Rus D (2020) Generating Visibility-Aware Trajectories for Cooperative and Proactive Motion Planning. In: 2020 IEEE International Conference on Robotics and Automation (ICRA), pp. 3220–3226, 2020. doi: 10.1109/ICRA40945.2020.9196809.

[7] Jaipuria N, Habibi G, How JP (2018) Learning in the Curbside Coordinate Frame for a Transferable Pedestrian Trajectory Prediction Model. In: 2018 21st International Conference on Intelligent Transportation Systems (ITSC), Maui, HI, pp. 3125-3131, 2018. doi: 10.1109/ITSC.2018.8569812.

[8] Singh KB (2019) Vehicle Sideslip Angle Estimation Based on Tire Model Adaptation. Electronics 8(2):199. doi: 10.3390/electronics8020199

[9] Tanenhaus M, Geis T, Carhoun D, Holland A (2010) Accurate Real Time Inertial Navigation Device by Application and Processing of Arrays of MEMS Inertial Sensors. In: IEEE/ION Position, Location and Navigation Symposium, Indian Wells, CA, pp. 20–26, 2010. doi: 10.1109/PLANS.2010.5507137.

[10] Perlmutter M, Robin L (2012) High-Performance, Low-Cost Intertial MEMS: a Market in Motion! In: Proceedings of the 2012 IEEE/ION Position, Location and Navigation Symposium, Myrtle Beach, SC, pp. 225-229, 2012. doi: 10.1109/PLANS.2012.6236884.

[11] Geng C, Mostefai L, Hori Y (2008) A Hybrid-like Observer of Body Slip Angle for Electric Vehicle Stability Control: Fuzzy Logic and Kalman Filter Approach. In: 2008 IEEE Vehicle Power and Propulsion Conference, Harbin, pp. 1–6, 2008. doi: 10.1109/VPPC.2008.4677425.

[12] Donald S, Corno M, Panzani G, M.Savaresi S (2017) Vehicle sideslip estimation: A kinematic based approach. Control Eng. Pract. 67:1-12.

[13] Gadola M, Chindamo D, Romano M, Padula F (2004) Development and Validation of a Kalman Filter-Based model for Vehicle Slip Angle Estimation. Vehicle Syst. Dyn. 52(1):68-84.

[14] Du H, Lam J, Cheung K-C, Li W, Zhang N (2015) Side-slip angle estimation and stability control for a vehicle with a non-linear tyre model and a varying speed. In: Proceedings of the Institution of Mechanical Engineers, Part D: Journal of Automobile Engineering, 229:486-505.

[15] Pi DW, Chen N, Wang JX, Zhang BJ (2011) Design and evaluation of sideslip angle observer for vehicle stability control. Int. J. Automot. Technol. 12:391-399.

[16] Tseng HE, Xu L, Hrovat D (2006) Estimation of Land Vehicle Roll and Pitch Angles. Vehicle Syst. Dyn., 45(5):433. doi: 10.1080/00423110601169713.

[17] Kojima Y (2010) Precise Localization using Tightly Coupled Integration based on Trajectory Estimated from GPS Doppler. In: Proceedings of AVEC 2010, 168:1-6.

[18] Takeyama K, Kojima Y, Teramot E (2012) Trajectory Estimation Improvement Based on Time-series Constraint of GPS Doppler and INS in Urban Areas. In: Proceedings of IEEE/ION PLANS 2012, pp. 700-705.

[19] POS-LV-Datasheet https://www.applanix.com/downloads/products/specs/POS-LV-Datasheet.pdf. Accessed 17 September 2020

[20] Serrano L, Kim D, Langley RB (2004) A GPS velocity sensor: How accurate can it be?—A first look. San Diego CA, pp.875-885, 2004

Figures

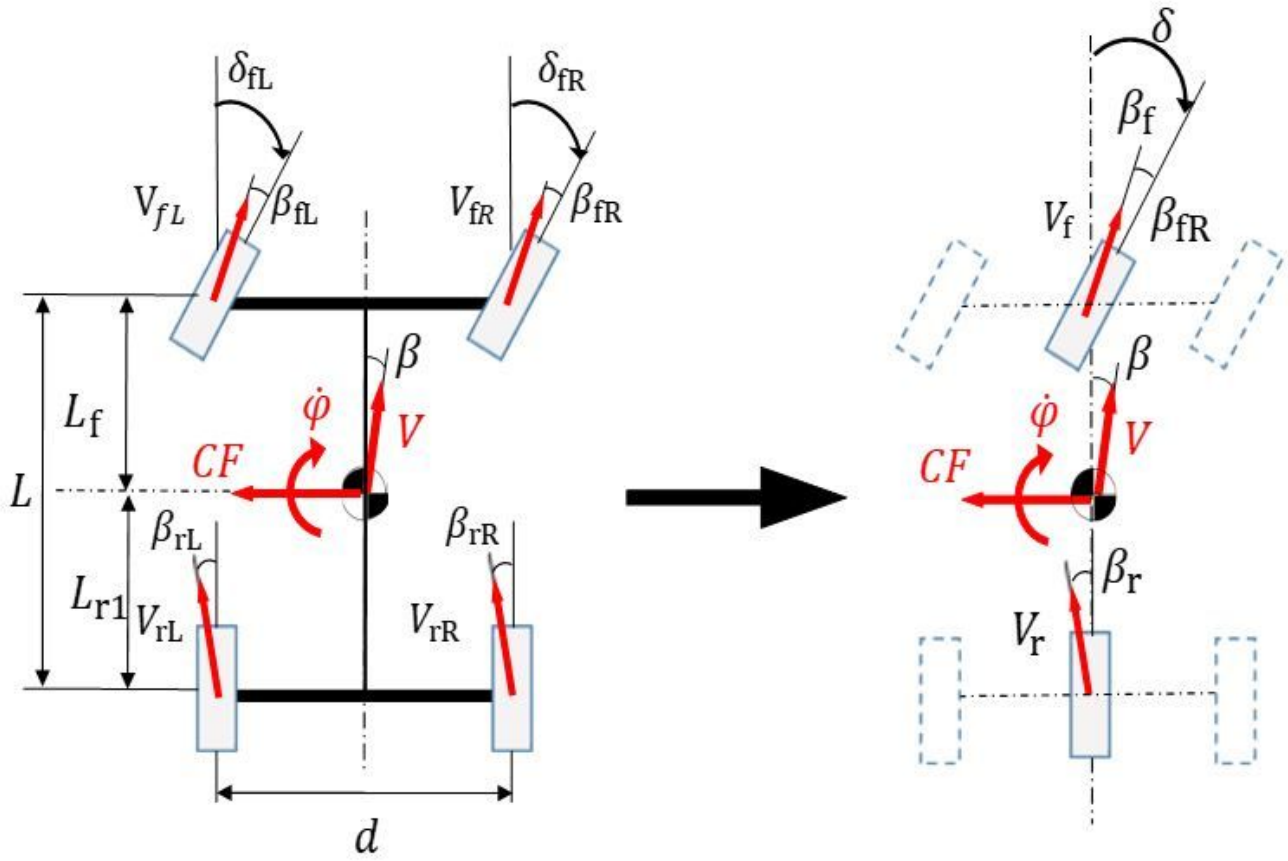

Figure 1

Two-wheel model

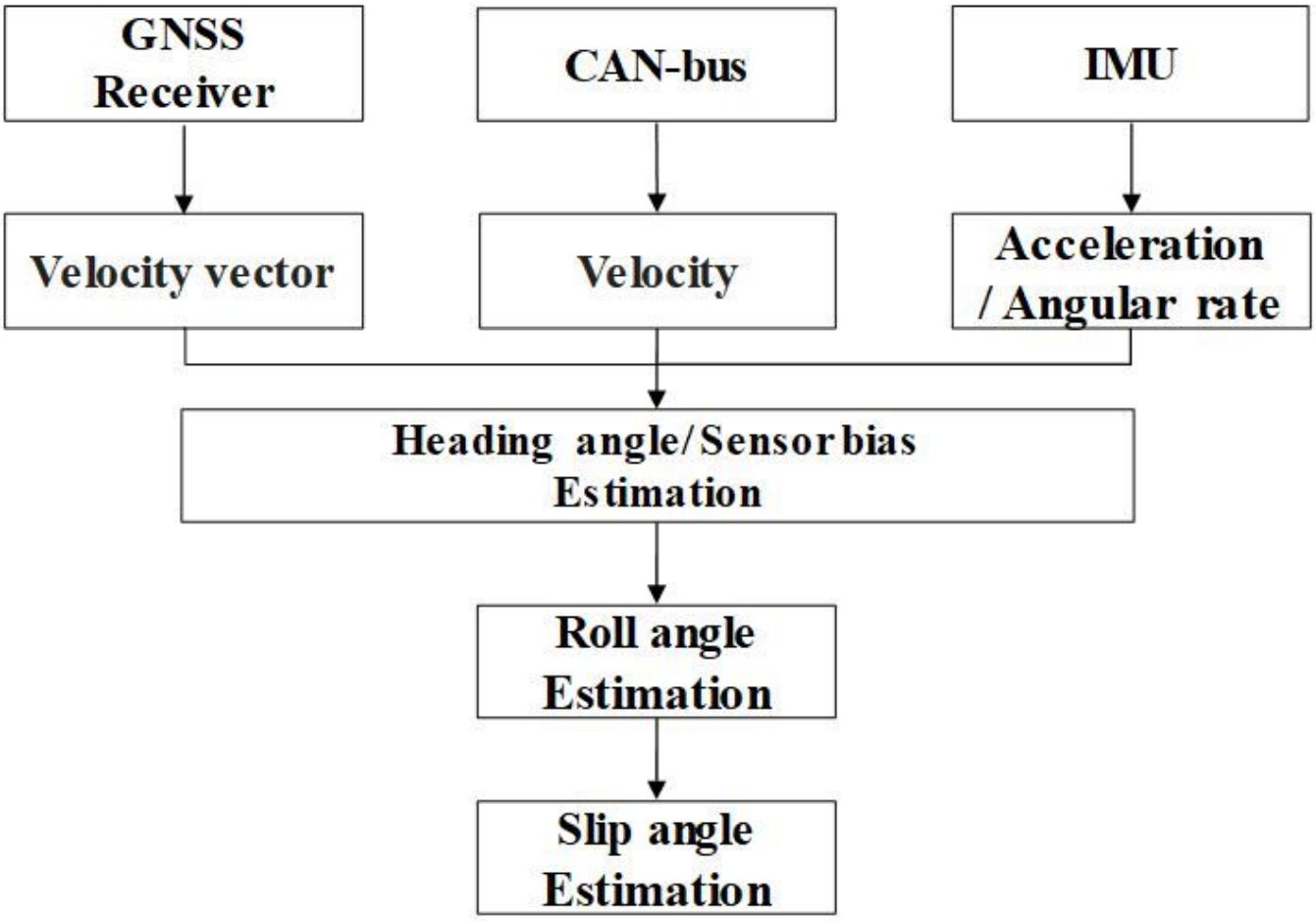

Figure 2

Overview of the proposal

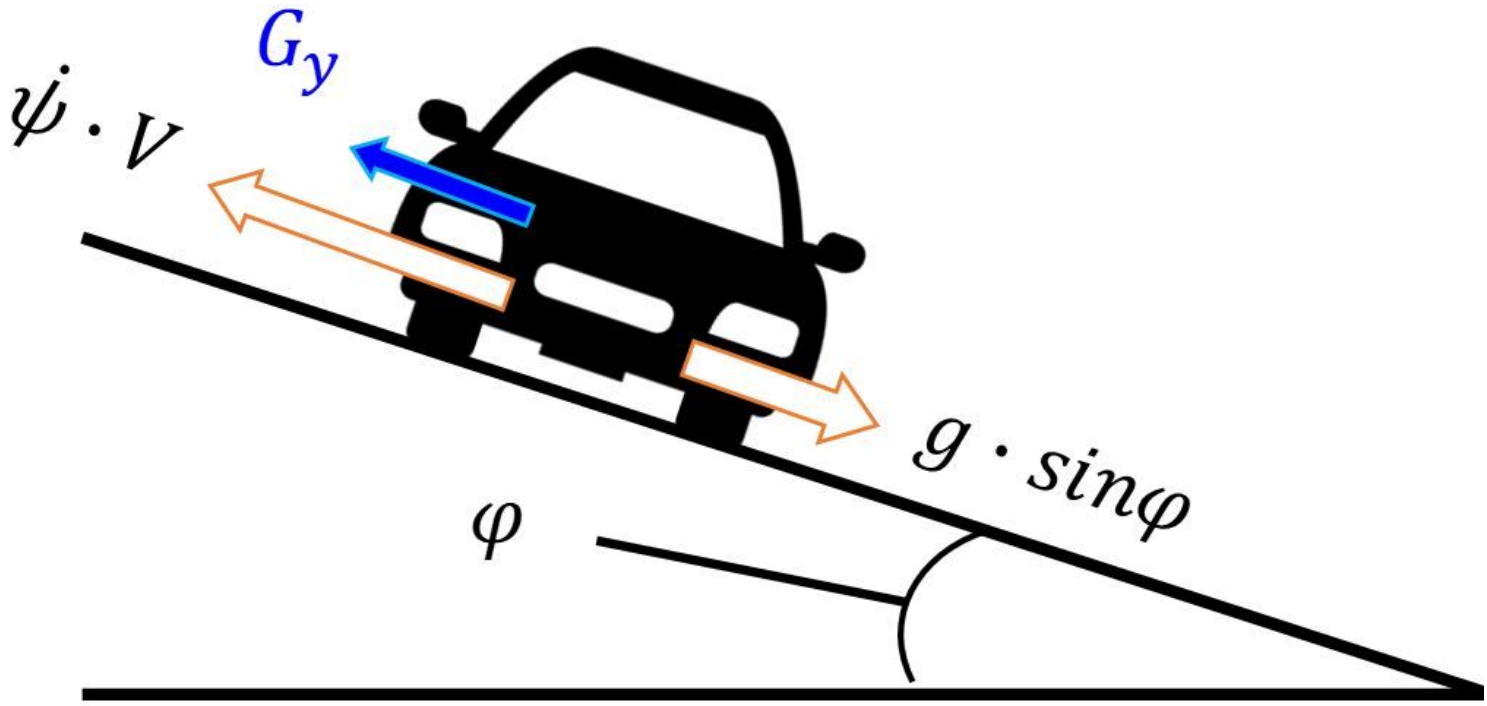

Figure 3

Effect of road lateral gradient

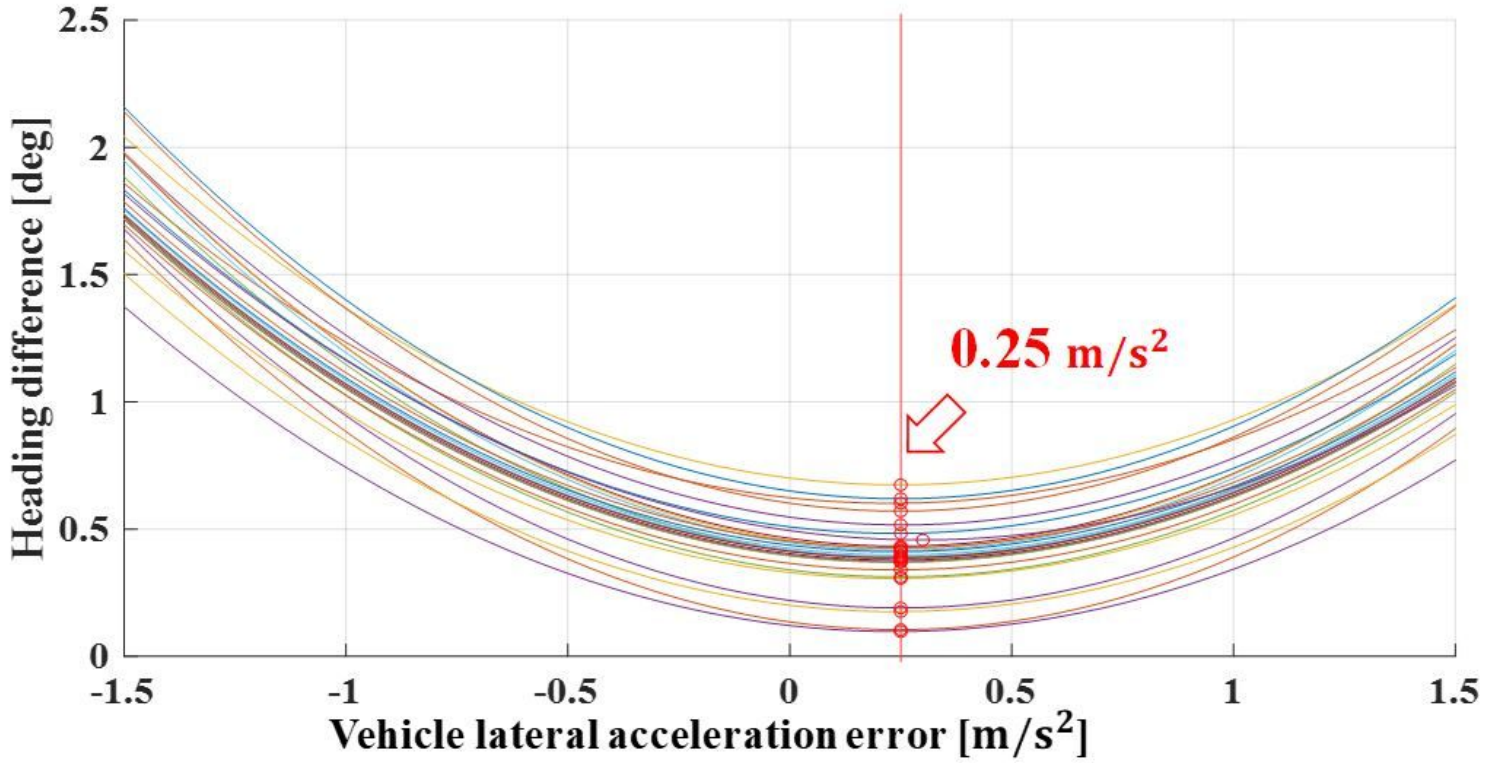

Figure 4

Estimation results of the lateral acceleration error

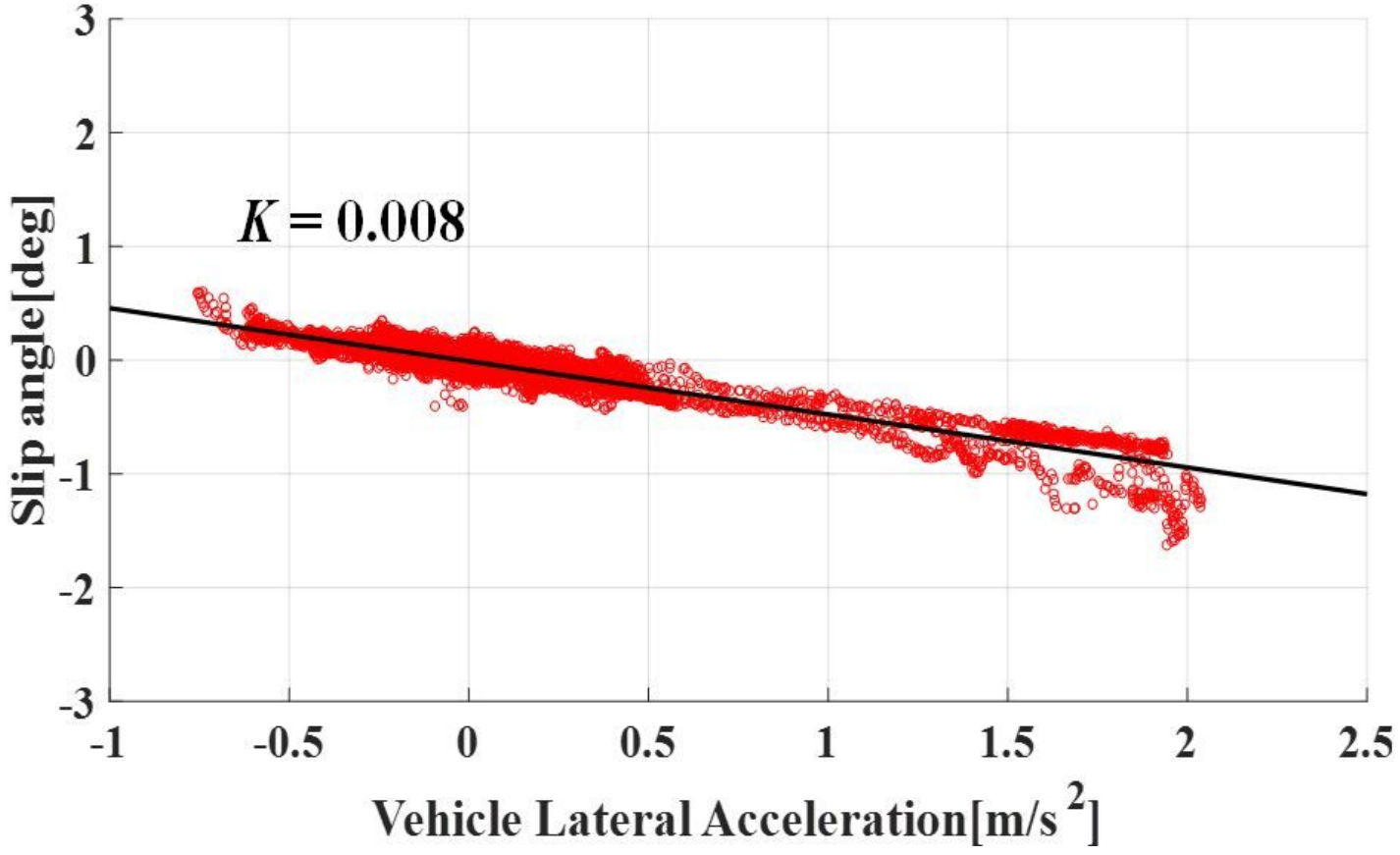

Figure 5

Correlation between slip angle and lateral acceleration (POSLV220)

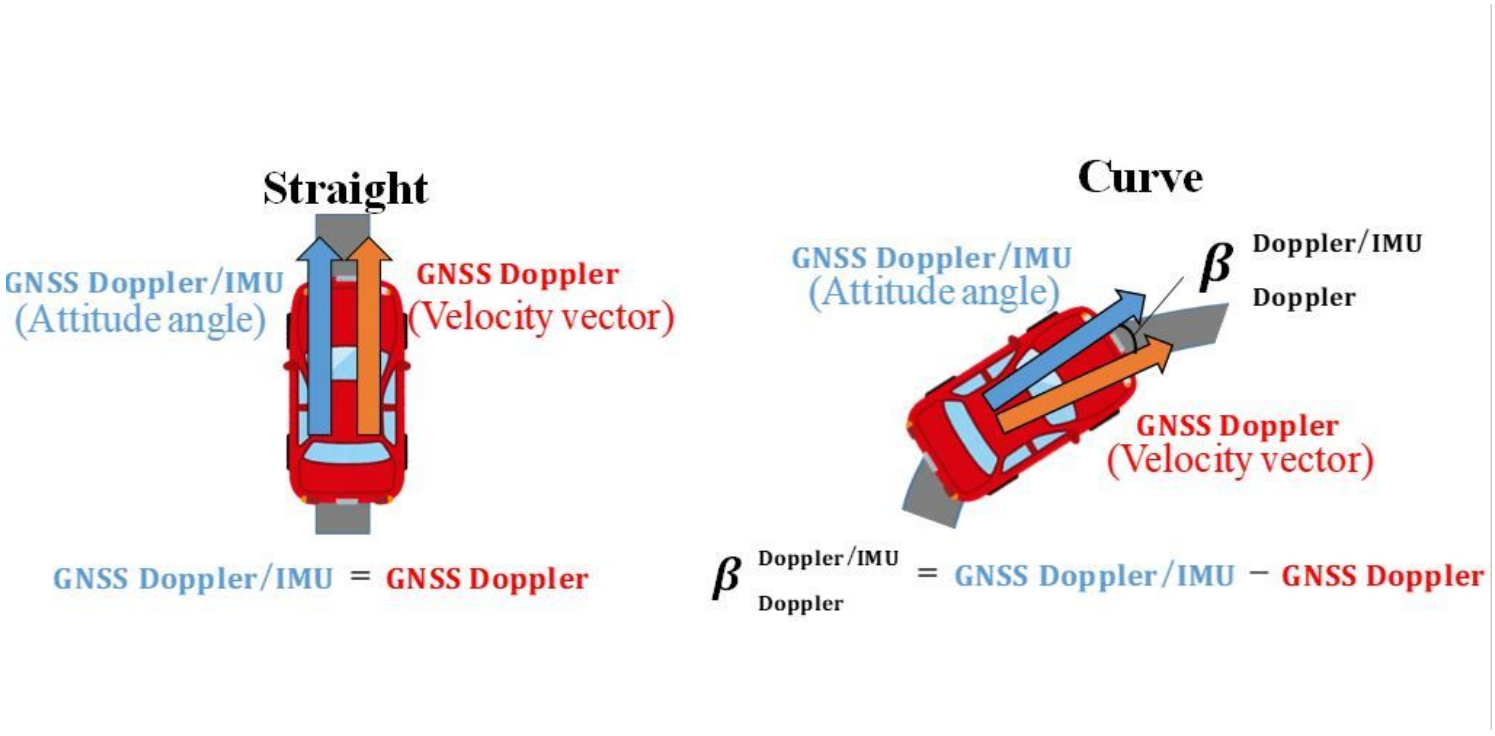

Figure 6

Overview of the slip angle

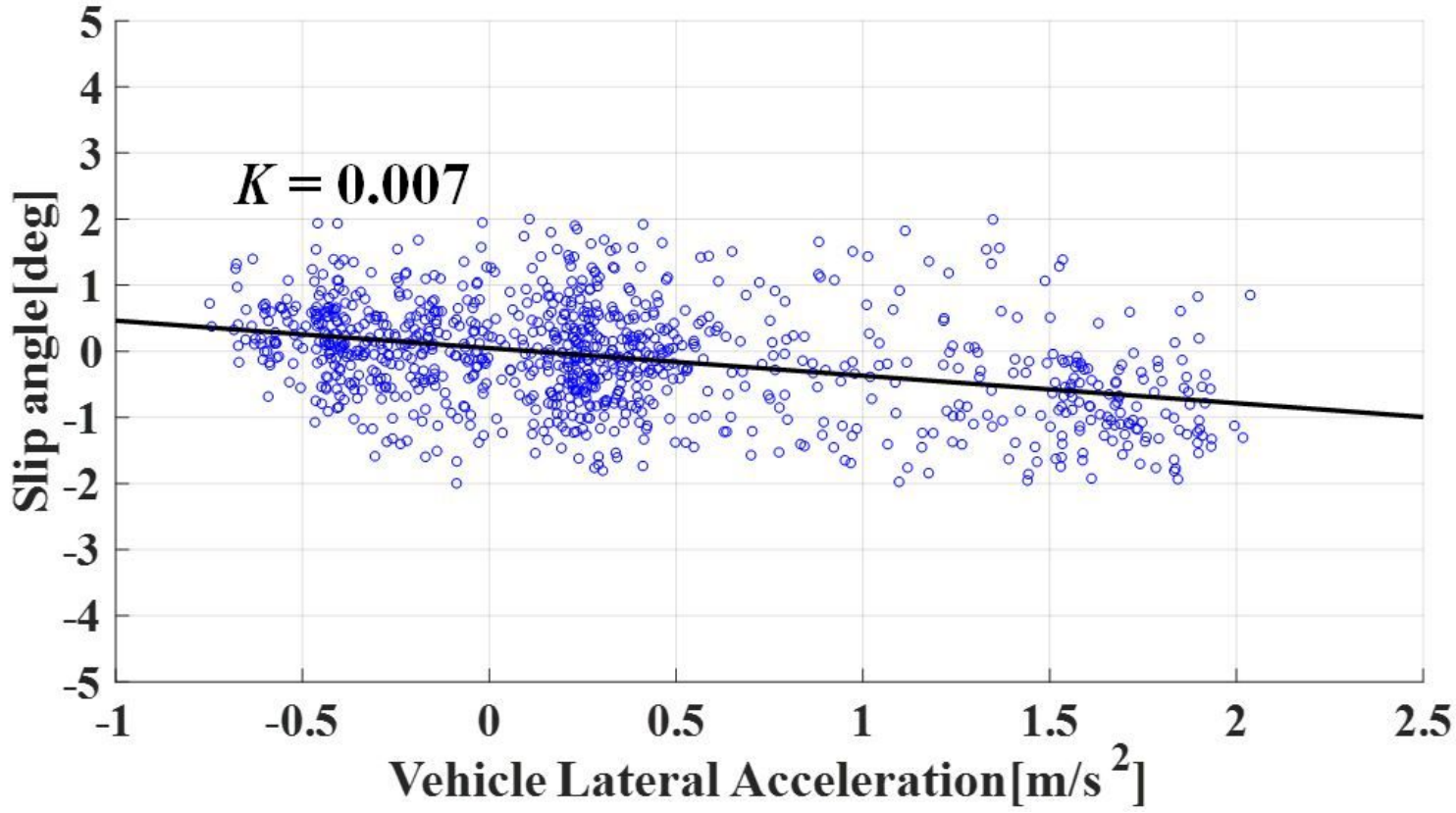

Figure 7

Relationship between slip angle and lateral acceleration using GNSS/Doppler

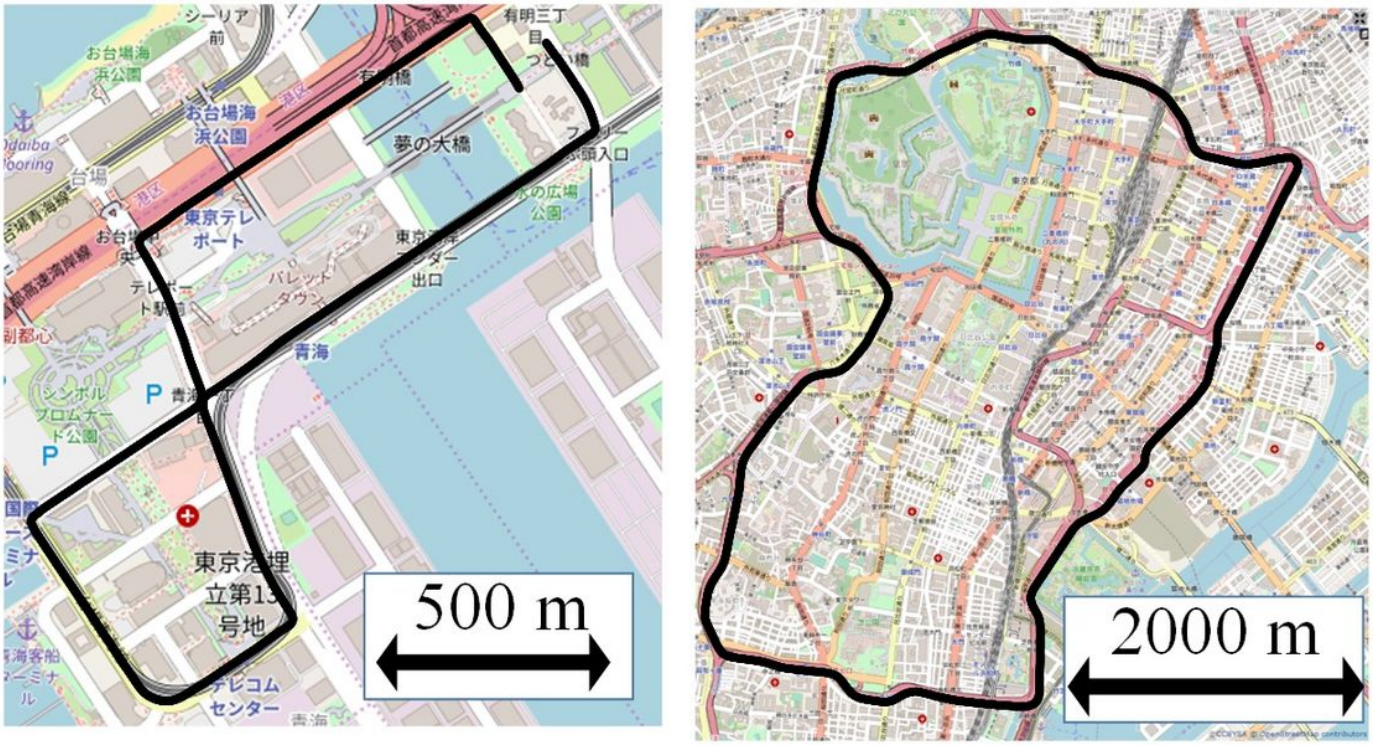

Figure 8

Evaluation fields [“© OpenStreetMaps”] Note: The designations employed and the presentation of the material on this map do not imply the expression of any opinion whatsoever on the part of Research Square concerning the legal status of any country, territory, city or area or of its authorities, or concerning the delimitation of its frontiers or boundaries. This map has been provided by the authors.

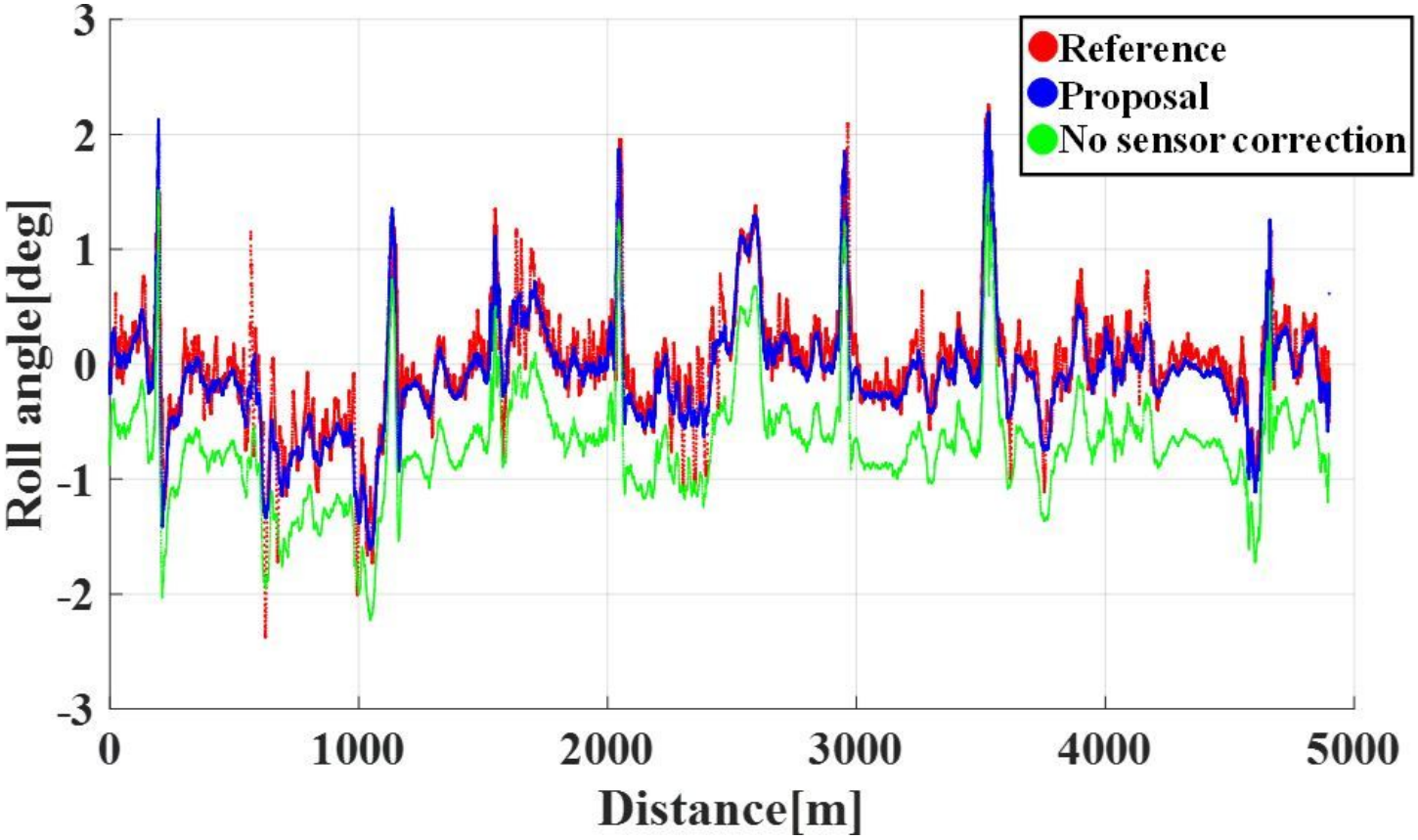

Figure 9

Estimated roll angle (Urban street)

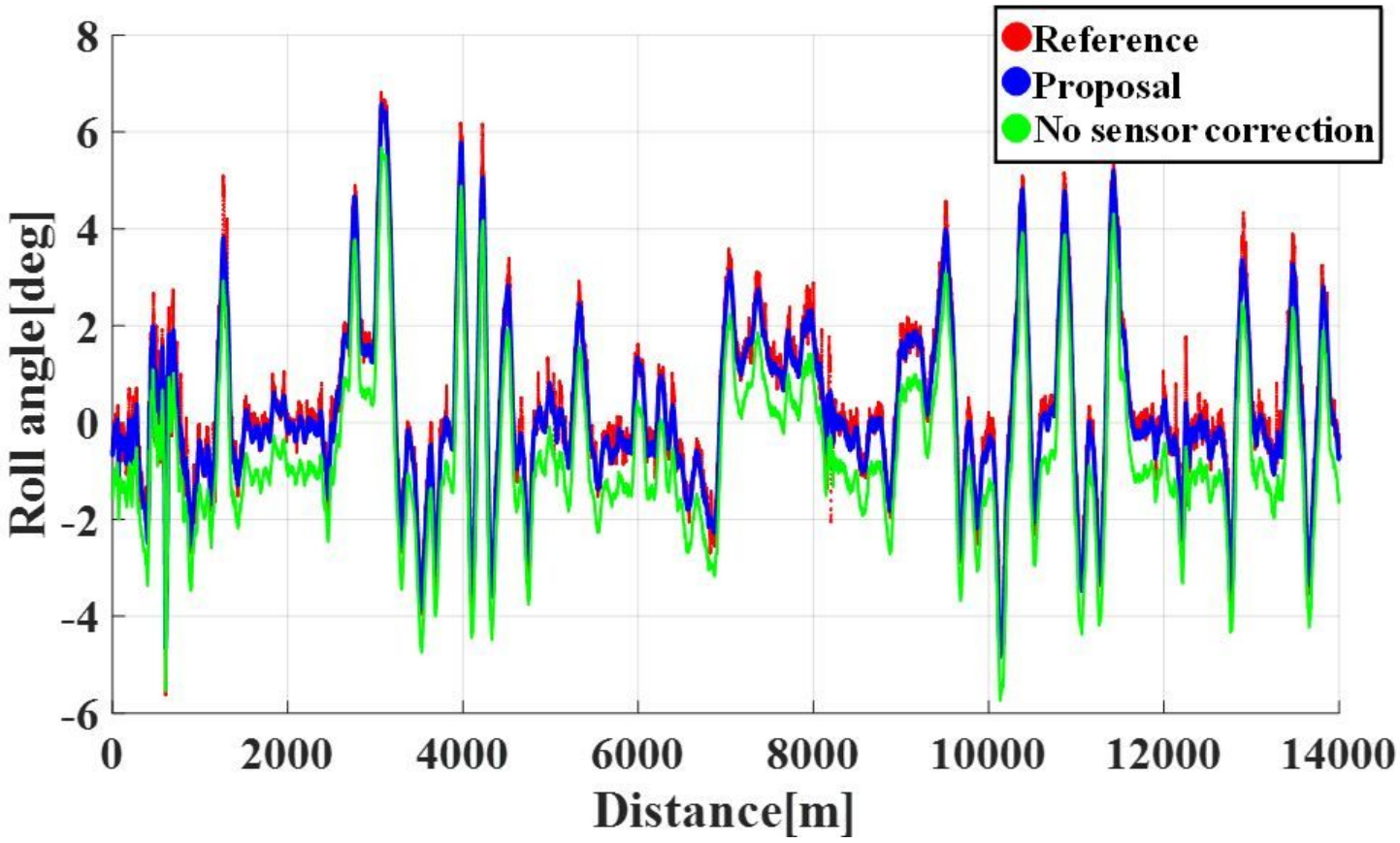

Figure 10

Estimated roll angle (Urban highway)

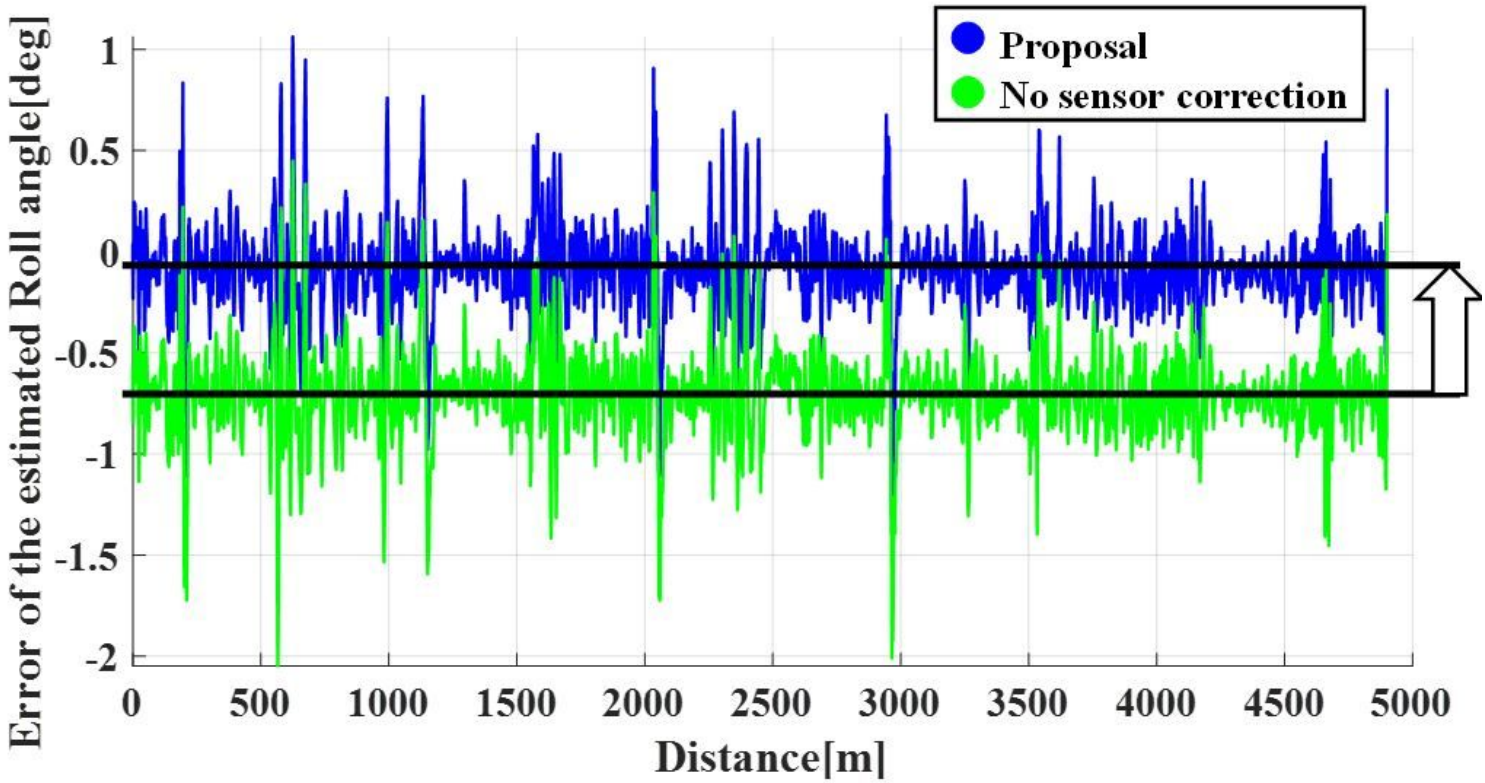

Figure 11

Error of estimated roll angle (Urban street)

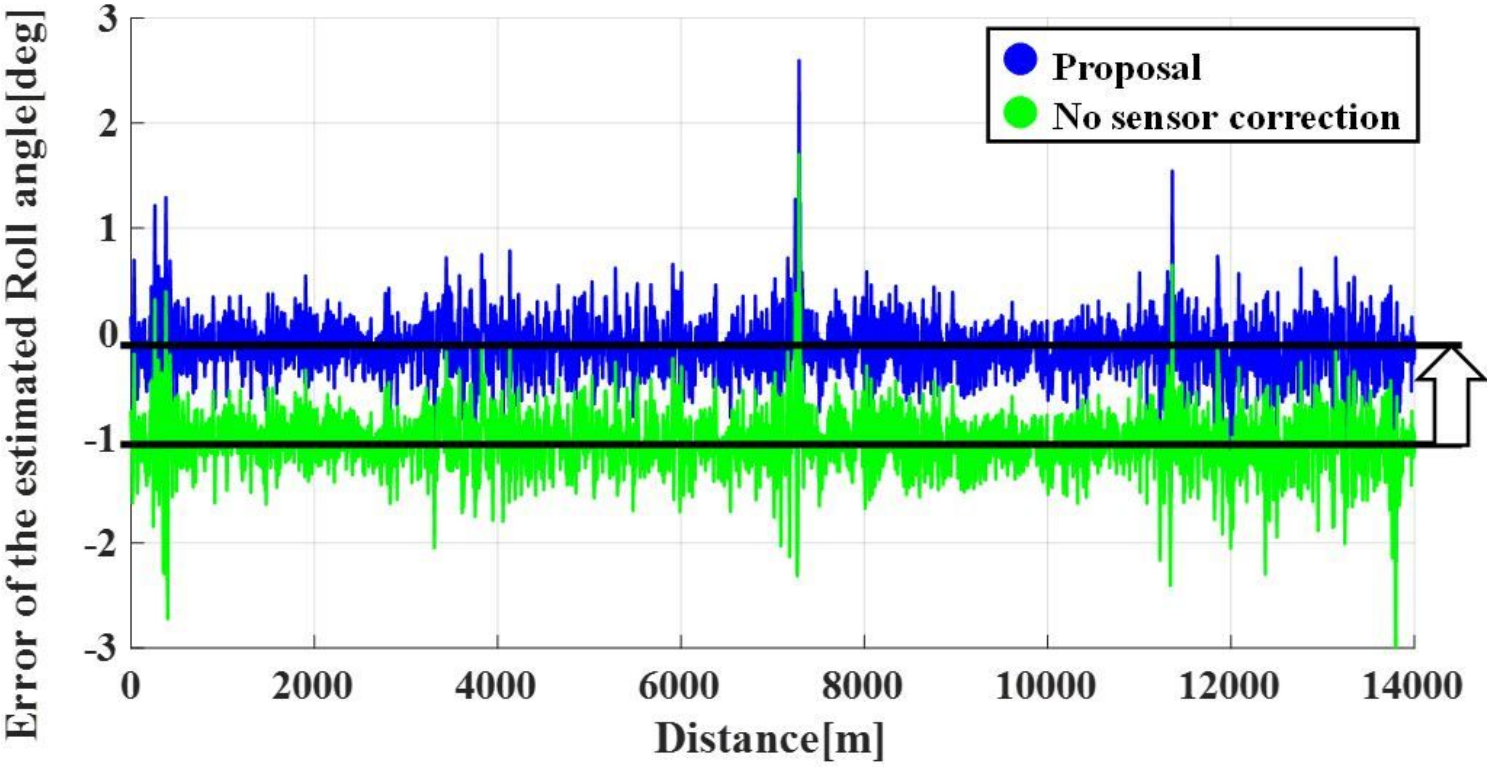

Figure 12

Error of estimated roll angle (Urban highway)

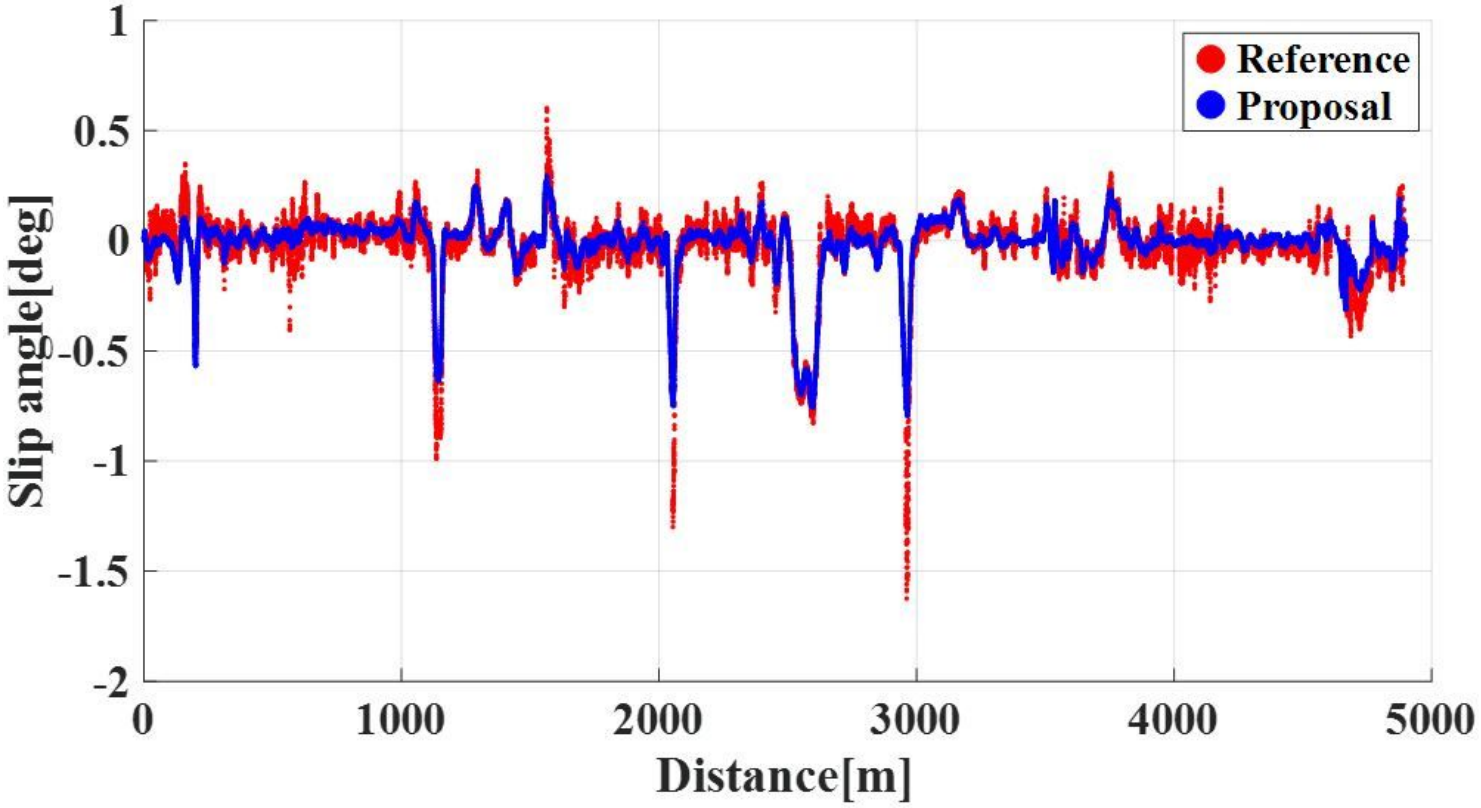

Figure 13

Estimated slip angle (Urban street)

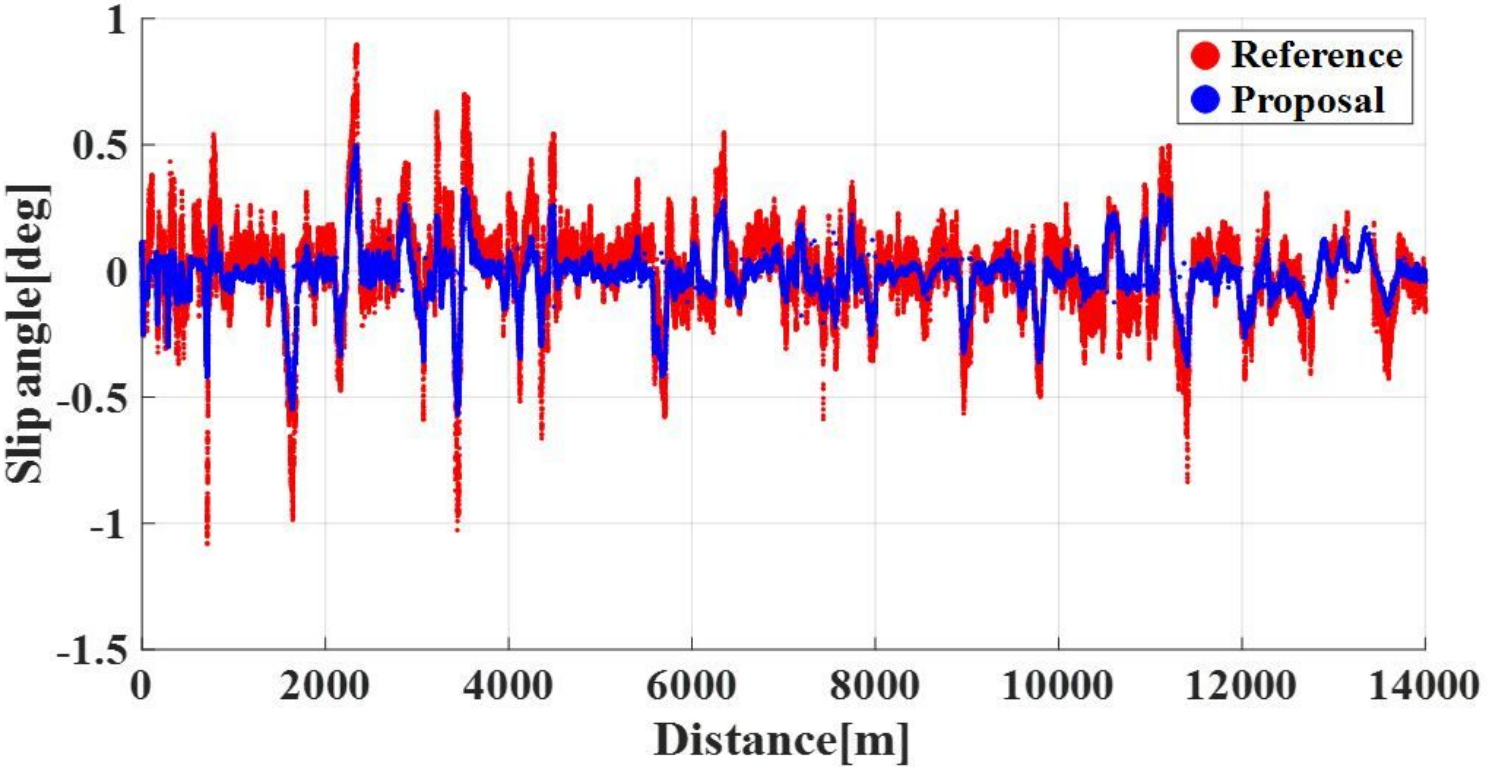

Figure 14

Estimated slip angle (Urban highway)

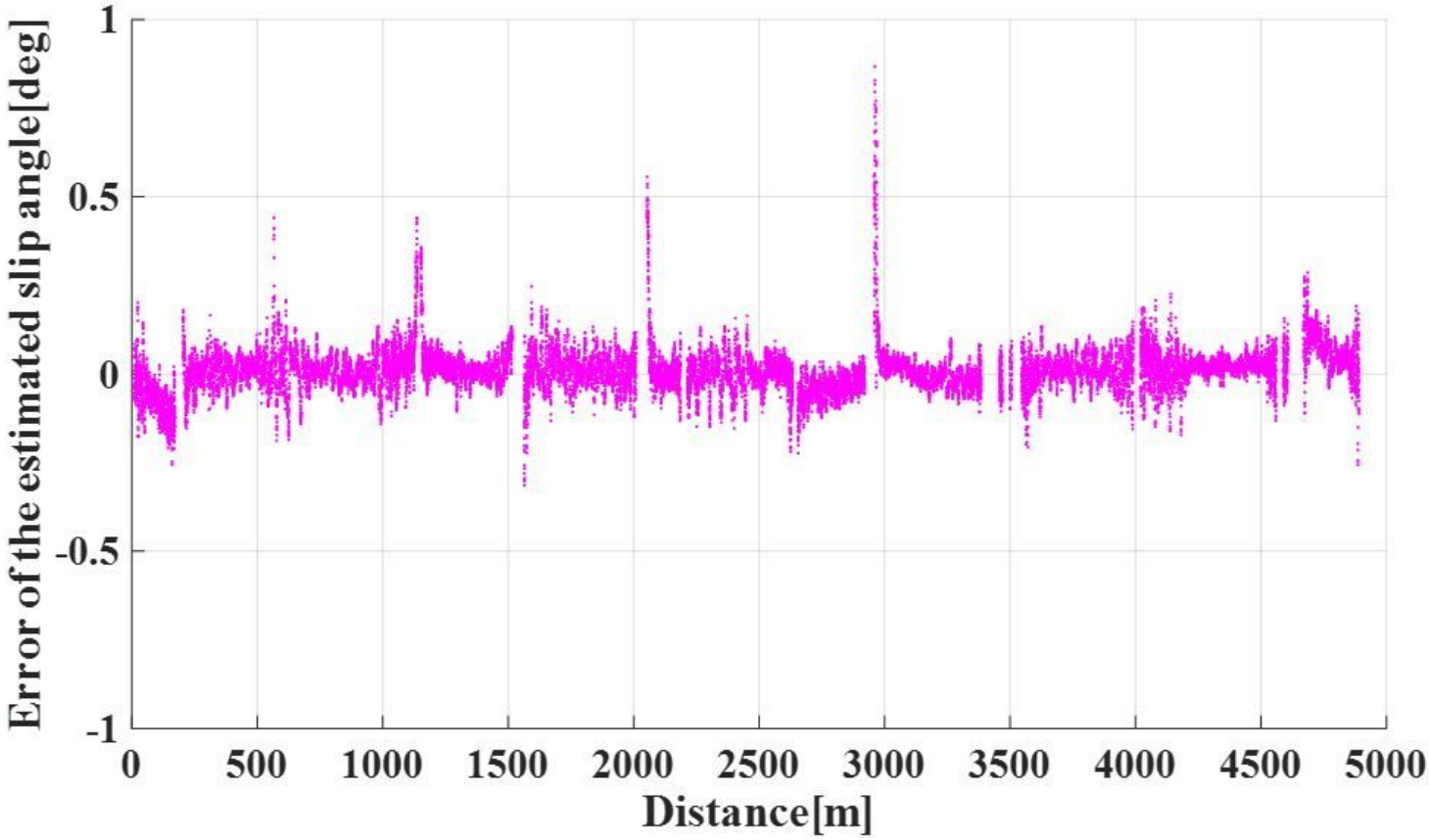

Figure 15

Error of estimated slip angle (Urban street)

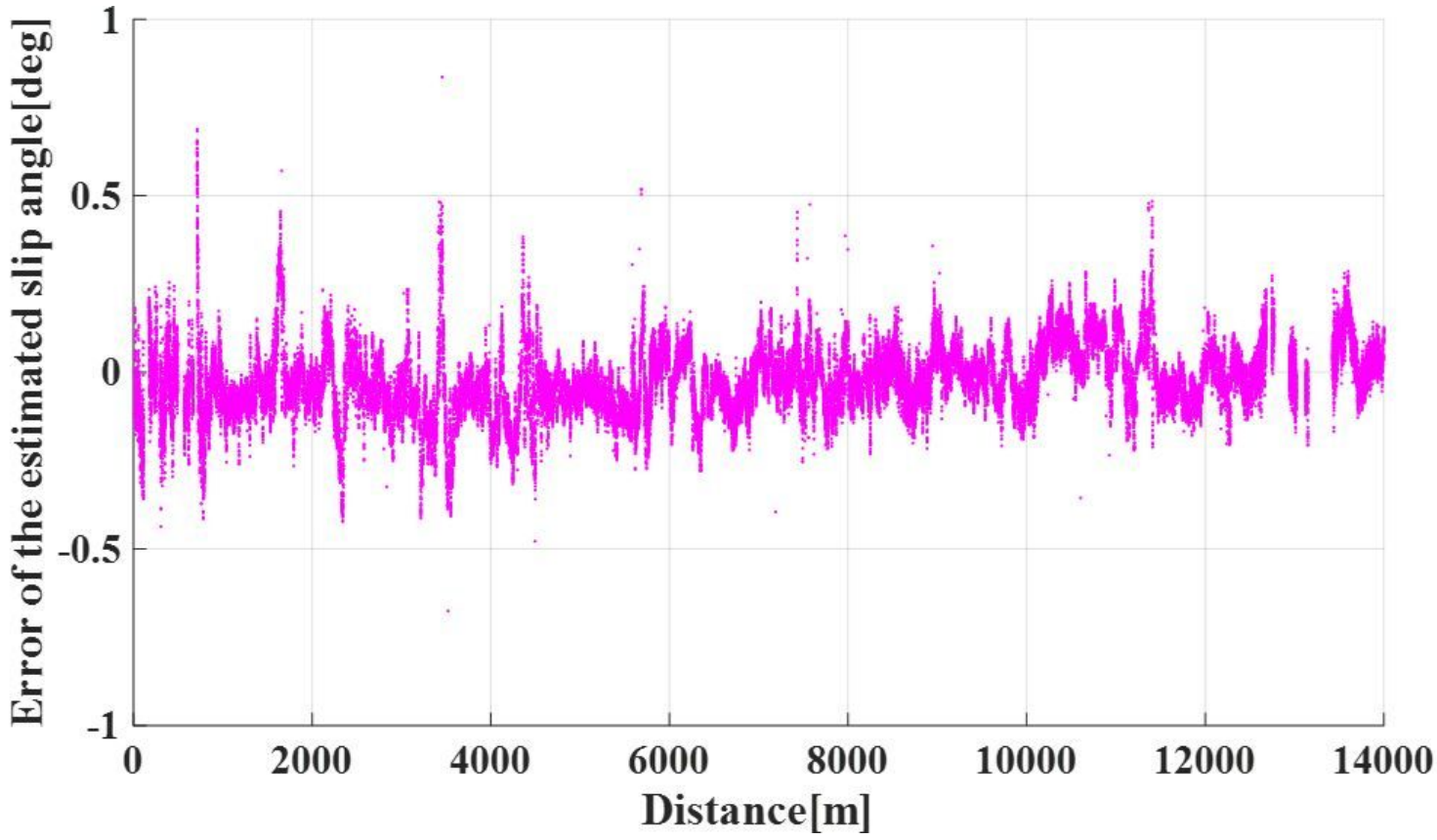

Figure 16

Error of estimated slip angle (Urban highway)

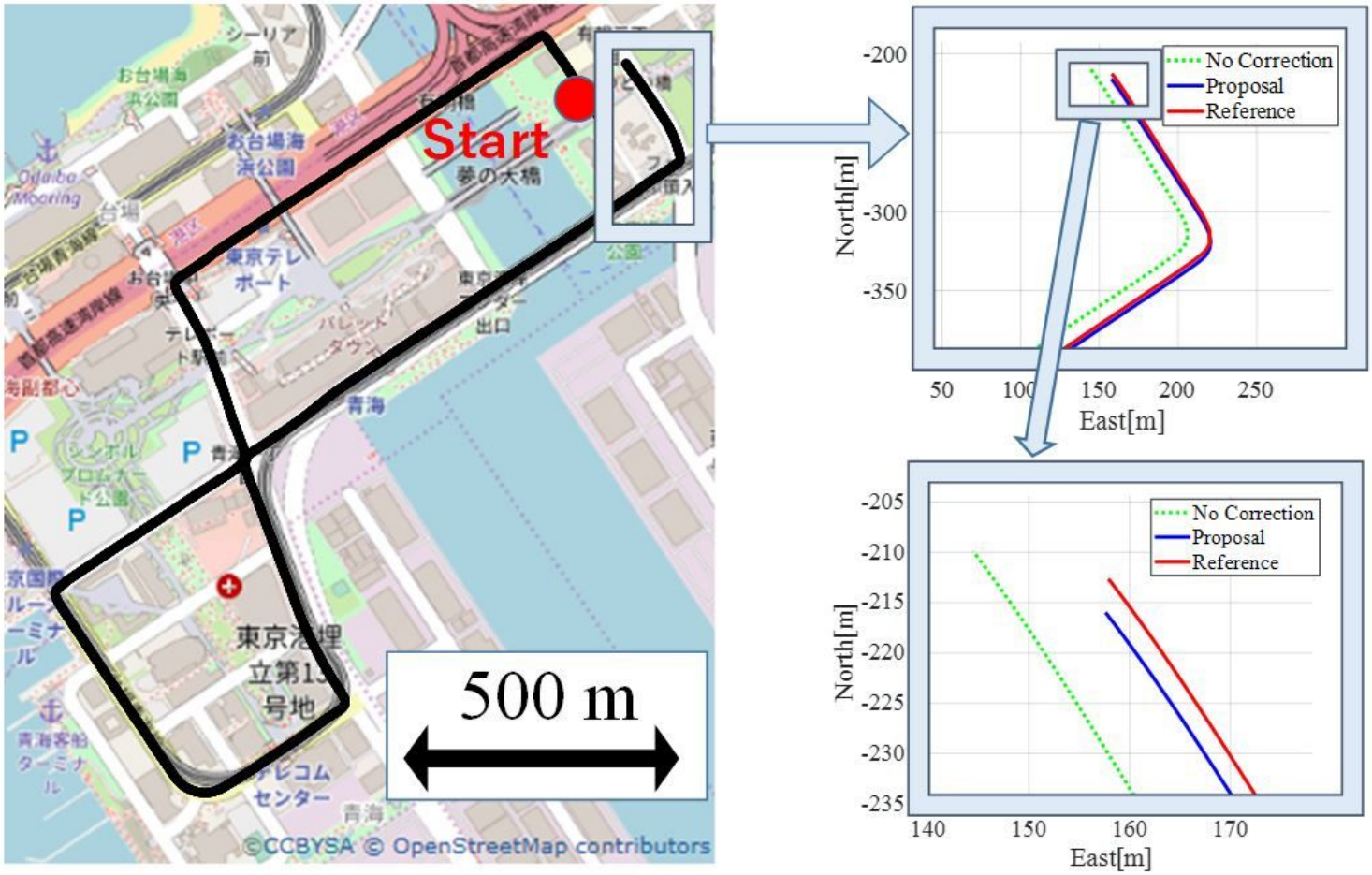

Figure 17

Effect of slip angle correction (Urban street) Note: The designations employed and the presentation of the material on this map do not imply the expression of any opinion whatsoever on the part of Research Square concerning the legal status of any country, territory, city or area or of its authorities, or concerning the delimitation of its frontiers or boundaries. This map has been provided by the authors.

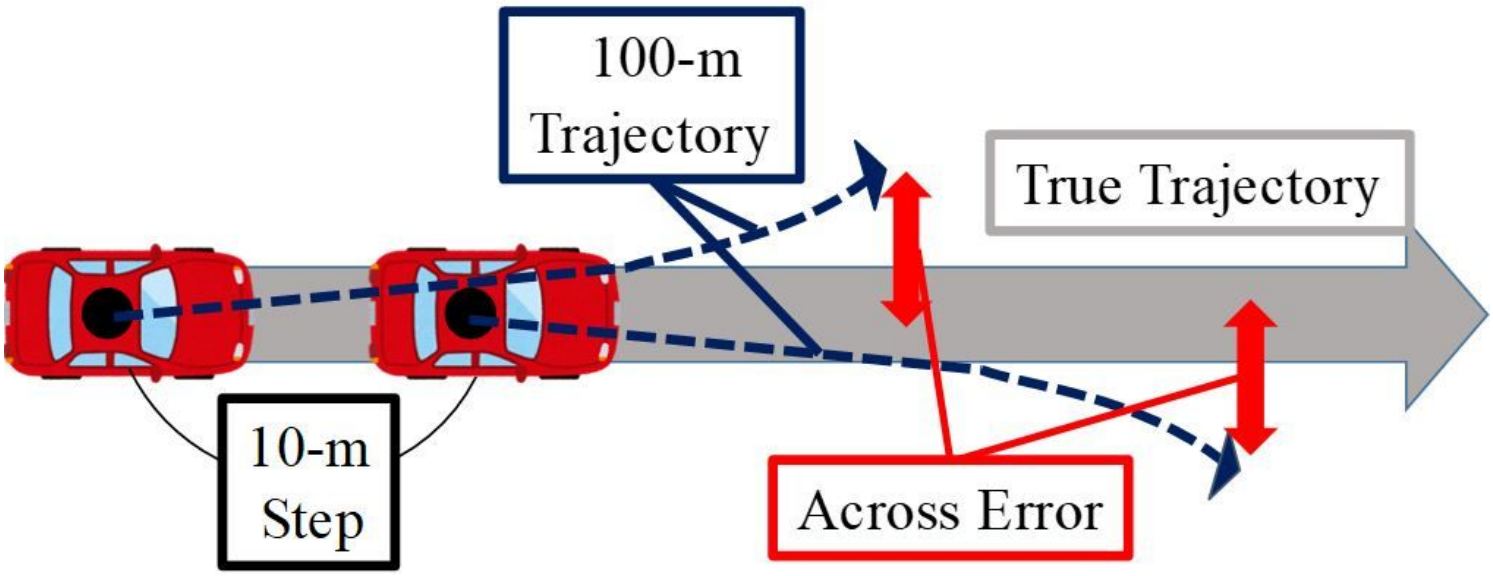

Figure 18

Overview of trajectory evaluation

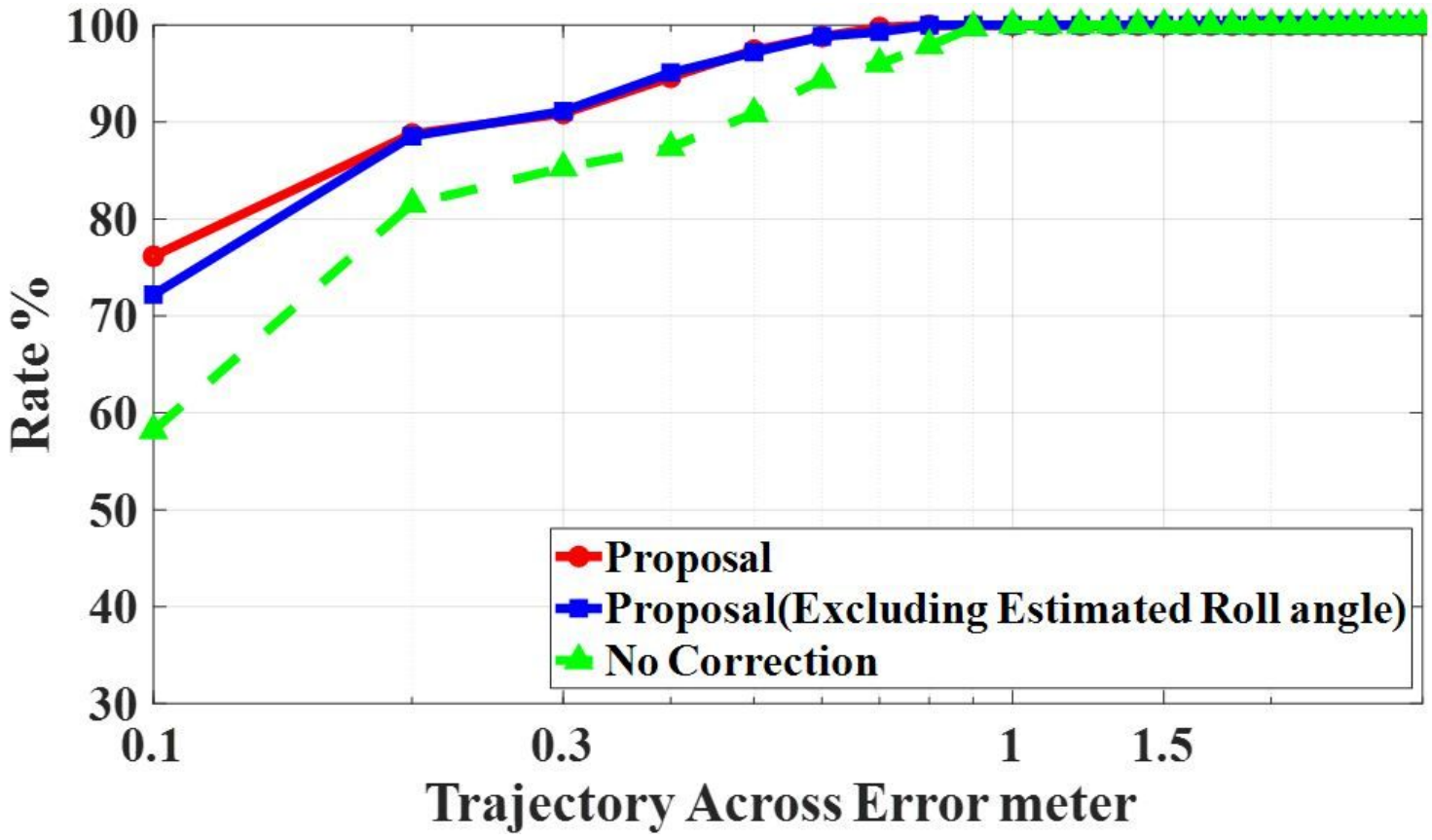

Figure 19

Evaluation of vehicle trajectory (Urban street)

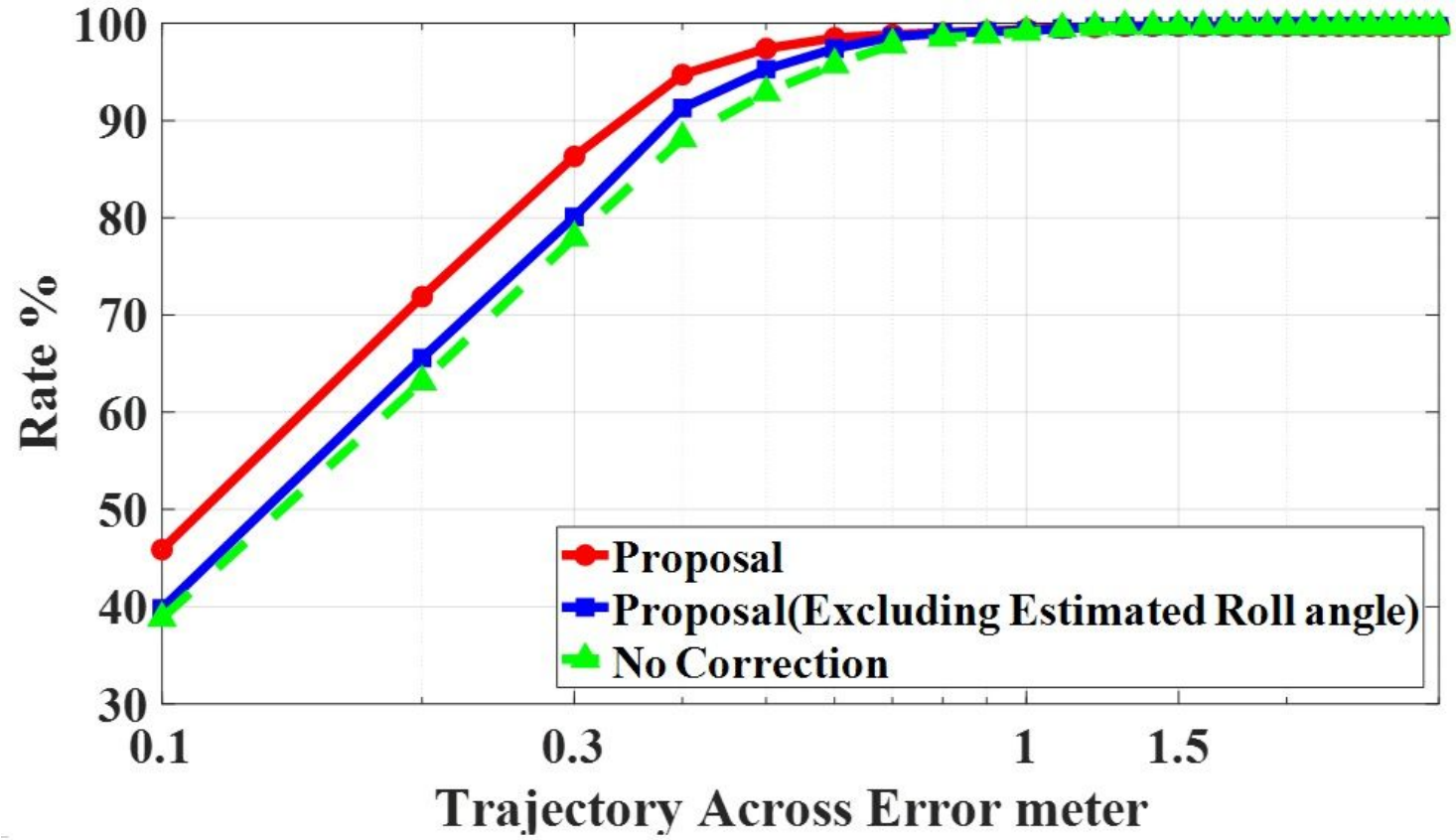

Figure 20

Evaluation of vehicle trajectory (Urban highway)